Reference : **APPL-06-2004**	*Version* : **1.1**	

Date : September 2004	*Nature* : Open	

Origin : Leila Fonseca (INPE) Flávio Ponzoni (INPE) Ricardo Cartaxo (INPE)	*Revised by* : José Carlos Epiphanio (INPE)

Authorized by : Luiz Carlos Miranda (INPE)	*Approved by* : Luiz Carlos Miranda (INPE)

Document Title

Radiometric Quality Assessment of CBERS-2

Distribution List

Company	To	Copies
CRESDA	Guo Jianning	1
CRESDA	Yu Jin	1
INPE	Luiz Carlos Miranda	1
INPE	Leonel Perondi	1
INPE	Gilberto Câmara	1
INPE	Janio Kono	1

DOCUMENT HISTORY

Version	History of Changes
1.0	Leila
1.1	Leila

1. Introduction

Two aspects must be considered in the image quality evaluation: geometrical and radiometric features. The image quality is evaluated during the so-called in-orbit test period, in order to verify if the subsystem requirements are complied with the specification and thus to obtain the image correction parameters to be used in the ground processing center. During the satellite's operational lifetime a complete quality assessment must be performed periodically and therefore, update the parameters if necessary.

This document aims to provide a preliminary radiometric quality assessment of CBERS-2. The radiometric image quality is directly related to the sensor performance. The radiometry of an image is satisfactory when the relationship between the ground reflectance of the target and the gray level of the pixel on the image are correct.

Usually, in the radiometric quality analysis the items to be checked are:

1. Signal to noise ratio (SNR)

   This parameter represents the camera radiometric resolution. It is the ratio of the measured signal to the overall noise at each detector.

2. Relative calibration

   The relative calibration allows to determining the gain and offset of each detector in order to correct the images.

3. MTF performance

   The modulation transfer function (MTF) corresponds to the sharpness of the image giving the response of the system to various spatial frequency of the scene. It is related to the sensor's spatial resolution.

4. absolute calibration accuracy

   The absolute calibration aims to convert the Digital Numbers (DN) of the TM images in physical data like radiance or reflectance.

5. Noises such as: loss of lines or columns in the image, striping effects, gray levels saturation, etc.

1. CCD Camera

CBERS-2 satellite carries on-board a multisensor payload with different spatial resolutions called: WFI (Wide Field Imager), IRMSS (Infrared MSS) and CCD (Charge Coupled Device) camera. CBERS-2 is technically identical to CBERS-1.

The high-resolution CCD Camera has 4 spectral bands from visible light to near infrared and one panchromatic band (Table. 1.1). It acquires the earth ground scenes by pushbroom scanning, on 778 km sun-synchronous orbit and provides images of 113 km wide strips with sampling rate of 20 meters at nadir. Since this camera has a sideways pointing capability of ± 32 degrees, it is capable of taking stereoscopic images of a certain region.

Table 1.1: Spectral bands of the CCD sensor.

Spectral Bands	Band	Wavelength (µm)
Blue	B1	0.45 – 0.52
Green	B2	0.52 – 0.59
Red	B3	0.63 – 0.69
Near-Infrared	B4	0.77 – 0.89
Pan.	B5	0.51 – 0.73

The signal acquisition system operates in two channels called CCD1 and CCD2. The first one generates images corresponding to B2, B3 and B4 while the second generates images corresponding to the bands B1, B3 and B5. In each channel (channel C1 and channel C2), three CCD arrays per band were combined to generate about 6000 pixels per row. A complete coverage cycle of the CCD camera takes 26 days.

1.1 Signal Noise Ratio

The specifications of signal noise ratio for CCD camera of CBERS-1 and CBERS2 are shown in the Table 1.1.1:

Table 1.1.1: Signal noise ratio and radiance for CBERS-2.

Band	Equivalent spectral Radiance (W/m2.Sr)		S/N (dB)	
	min	max	min	max
B1	4.6	28.7	32	48
B2	3.7	30.1	31	50
B3	2.4	25.9	26	48
B4	2.7	35.6	29	52
B5	9	55.6	37	53

The randon noise level measured was 2.7 mV that is equivalent to about 0.7 DN. Table 1.1.2 shows the signal noise rate and radiance level measured in the laboratory.

Table 1.1.2: Spectral radiance and signal noise ratio.

Band	Equivalent spectral Radiance (W/m2.Sr)		S/N (dB)	
	min	max	min	max
B1	2.7	22.0	28	46
B2	1.8	22.4	33	55
B3	1.1	19.4	25	50
B4	1.2	29.5	25	53
B5	4.8	46.9	37	57

One has observed that band 1, band 3 and band 4 presented the signal noise ratio 4 db, 2 db and 1 db, respectively, lower than those specified. Besides, the maxima spectral radiance values for all bands are lower than specifications. Therefore, saturation level is reached for a spectral radiance level lower than the one specified.

One also has observed (CAST) that the spectral band B2 range is broader than one specified as shown in table below:

specification	measurement
0.52 – 0.59 µm ±10 nm	0.515 – 0.635 µm ±10 nm

The broadening of band 2 occurred due to technical difficulties in meeting the project specification by CAST. The wider the spectral band the greater the radiance in the detector, which decreases the instrument dynamic range in the spectral band. Thus, the saturation level is reached for a spectral radiance level much lower than the one expected. Different combinations of sun elevation angle and target reflectance define the saturation level. The best situation for band 2 in terms of sun illumination (a=70 graus) is when the maxima reflectance is about 0.33.

1.2 Gray level Saturation

CCD images of band 4 have presented high contrast and brightness in relation to bands 1, 2 and 3 and in some cases the DN values are saturated. Figure 1.2.1 shows the histograms for band 2, 3 and 4 of CBERS-2 and TM of a region of São Jose dos Campos for sensors TM-5, SPOT-3, CBERS-1 and CBERS-2. One can observe that only images of CBERS-2 (30-01-2004, path/row 163-126) in the band 4 presents high average gray level and contrast (Table 1.2.1 and Figure 1.2.1).

Table 1.2.1: Mean and standard deviation (contrast) values.

| Band	Band 2		Band 3		Band4	
Sensor	mean	Deviation	mean	Deviation	mean	deviation
CBERS-1 CCD	48.78	3.65	60.40	8.53	84.39	7.70
CBERS-2 CCD	79.56	20.74	35.30	13.17	165.7	24.64
SPOT-3	75.79	12.90	46.85	11.34	75.38	11.6
TM-5	37.23	9.66	43.92	19.31	71.10	19.6

The saturation problem is common in the images of agriculture and urban areas which have high reflectance level in band 4. One way to solve this problem is changing the detector gain (actual configuration gain =1.0). In this case all bands in the same channel (C1={2, 3a and 4} or C2={1, 3b and 5}) will be affected since the gain is the same for individual channel. The possible 4 gain values are: 0.59 ; 1.0; 1.69 and 2.86.

The contrast stretching(Figure 1.2.2) in order to balance the color (similar mean and variance values) sometimes can lead to the gray level saturation, reducing the data quality.

In accord to "Cbers CCD Camera (FM2) Test Report" the bands Band2 and Band5 saturate at values lower than the maximum value specified in the project (Table1.2.2) whereas band 5 will saturate in any condition. Therefore, for targets with high responses in these bands will certainly lead to saturation.

Table 1.2.2 : maximum reflectance, for zenital sun angle = 20 graus.
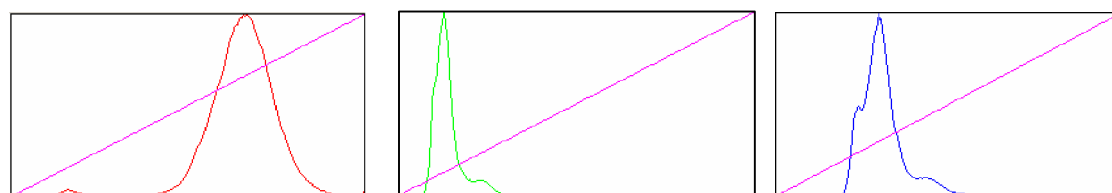
	max reflec	saturation	gain	reduce saturation
banda2	0.7	0.33	1.0	0.59
banda4	0.5	0.7	0.59	in the limit
banda5	0.5	0.33	1.0	saturate anyway
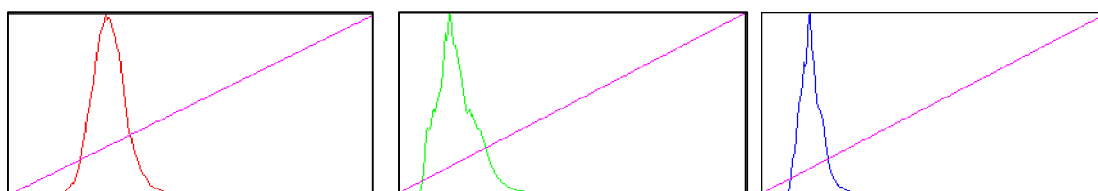
(a) TM
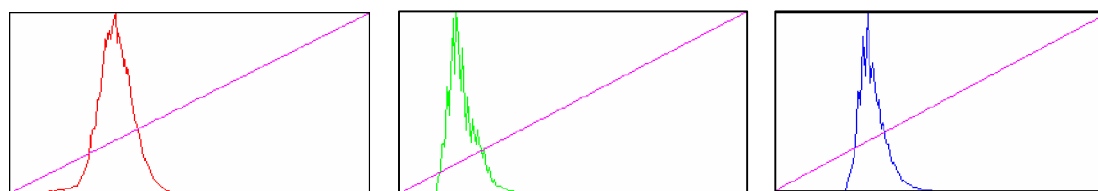
(b) SPOT-3

(c) CBERS-2
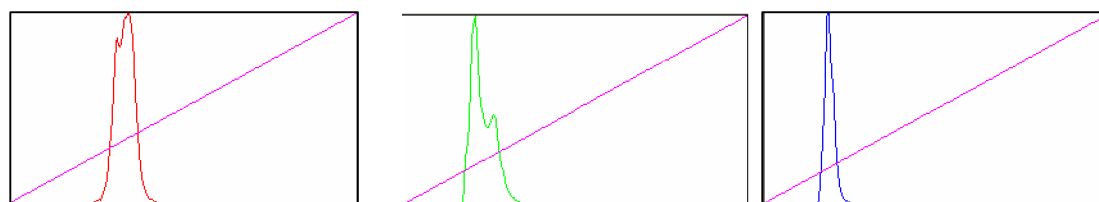
(d) CBERS-1

Figure 1.2.1 – Histograms of bands 4, 3 and 2 fom left to right for (a) TM-5, (b) SPOT-3, (c) CBERS-2 and (d) CBERS-1.
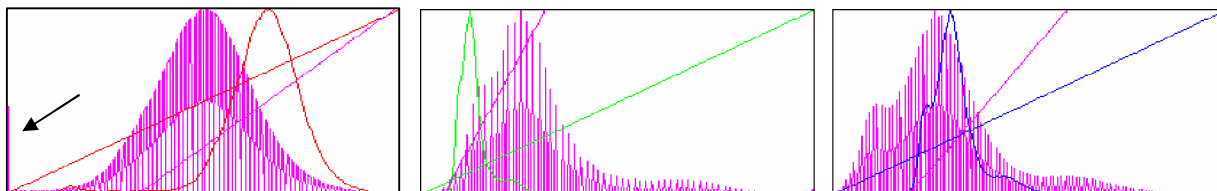
Figure 1.2.2 — Histogram stretching of bands 4, 3 and 2 for CBERS-2.

1.3 Correlation

The CBERS-2 CCD correlation coefficient for Bands 2 and 3   is high. The same was observed for bands B2 and B3 of TM-5 and SPOT-3 sensors.   Examples of two images of urban areas such as, Ribeirão Preto (date: 2003-11-04 path/row: 156/124) and São Jose dos campos (date: 2004-01-30   path/row: 153_126), illustrate this fact.

CBERS-2 (Ribeirão preto)

	B2	B3	B4
B2	1.00	0.93	0.35
B3	0.93	1.00	0.15
B4	0.35	0.15	1.00

CBERS-2 São Jose dos Campos

	B2	B3	B4
B2	1.00	0.93	0.57
B3	0.93	1.00	0.47
B4	0.57	0.47	1.00

TM-5 (são Jose dos Campos)

	B2	B3	B4
B2	1.00	0.98	0.78
B3	0.98	1.00	0.74
B4	0.78	0.74	1.00

SPOT-3 (São Jose dos Campos)

	B1	B2	B3
B1	1.00	0.53	0.65
B2	0.53	1.00	0.95
B3	0.65	0.95	1.00

1.4 Modulation Transfer Function (MTF) estimation

One way to evaluate the radiometric quality of a sensor is through its spatial resolution measurement. The spatial response can be determined in terms of the Point Spread Function (PSF) or Modulation Transfer Function (MTF).

The modulation transfer function (MTF) of an imaging system is of fundamental importance in both the initial specification and design of the system and in subsequent detailed analysis of the images it produces. Other important parameter is the Effective Instantaneous Field of View (EIFOV), which is used

to measure the system performance and it is defined as a function of the MTF (modulation transfer function) of the sensor. EIFOV is defined as a function of the frequency in which the MTF is equal to 50% of its maximum value (Figure). The EIFOV parameter enables a comparison between different sensors with similar nominal spatial resolution.
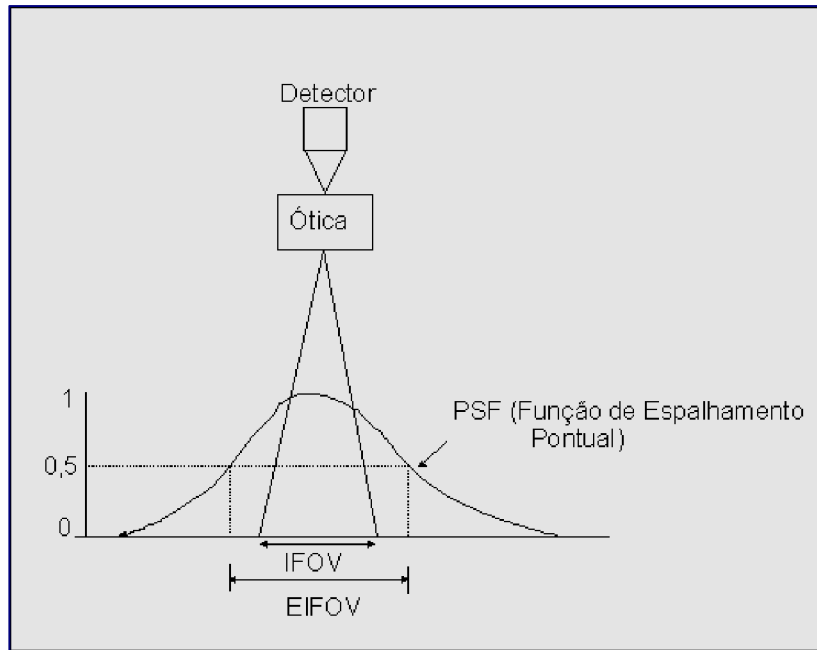

Figure 1.4.1 – EIFOV definition.

The MTF measurement in acroos-track direction was obtained in laboratory. MTF values were measured for 4 frequencies values (38.5 ; 19.25; 14.9 and 12.8 pl/mm). The nyquist frequency is 38.5 pl/mm. Table 1.4.1 and Figure 1.4.2 shows the MTF values.

Table 1.4.1: MTF values obtained in laboratory.

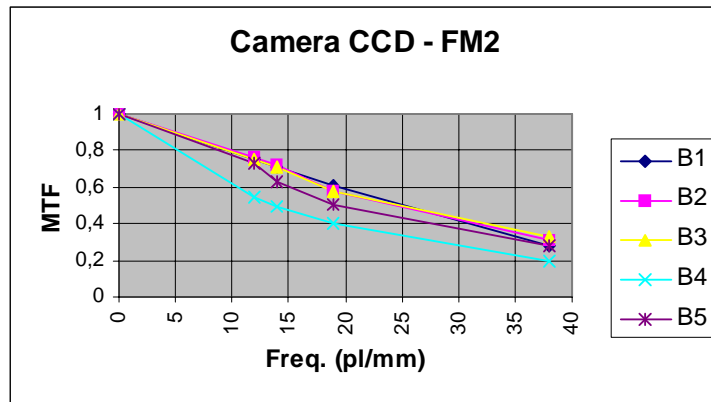| Freq. (pl/mm)	MTF				
	B1	B2	B3	B4	B5
12.8	0.75	0.76	0.75	0.55	0.73
14.9	0.71	0.72	0.71	0.50	0.63
19.25	0.61	0.51	0.58	0.40	0.51
38.5	0.28	0.31	0.33	0.20	0.28

Camera CCD - FM2

Figure 1.4.2 – MTF values measured in laboratory.

Band 4 presents MTF value in the nyquist frequency equal to 0.20 which is worse that the specification value ($\geq$ 0.28 in across-track direction and $\geq$ 0.18 in the along–track direction). Based on MTF values obtained in the laboratory, the EIFOV values are calculated (Table 1.4.2).

Table 1.4.2: EIFOV values before launching.

Band	EIFOV (m)
B1	30.4
B2	31.0
B3	31.0
B4	53.0
B5	38.0

CCD on-orbit modulation transfer function (MTF) estimation has been performed using images of ground targets such as bridges. The experiments have used images of Pontchartrain Lake bridge in Louisiana (25-09-2004 and path/row:211-66) , Rio-Niteroi bridge (10/07/2004 and path/row:151-126), a bridge in the the Bay Saint Louis and a bridge in Ilha Solteira (30/08/2004 and path/row:160-123). Images of bridges used in the experiments are illustrated in Figures 1.4.3 to 1.4.6.

Figure 1.4.3 – Saint Louis bridge.

Figure 1.4.4 – Rio Niterói bridge (10/07/2004 and path/row:151-126).

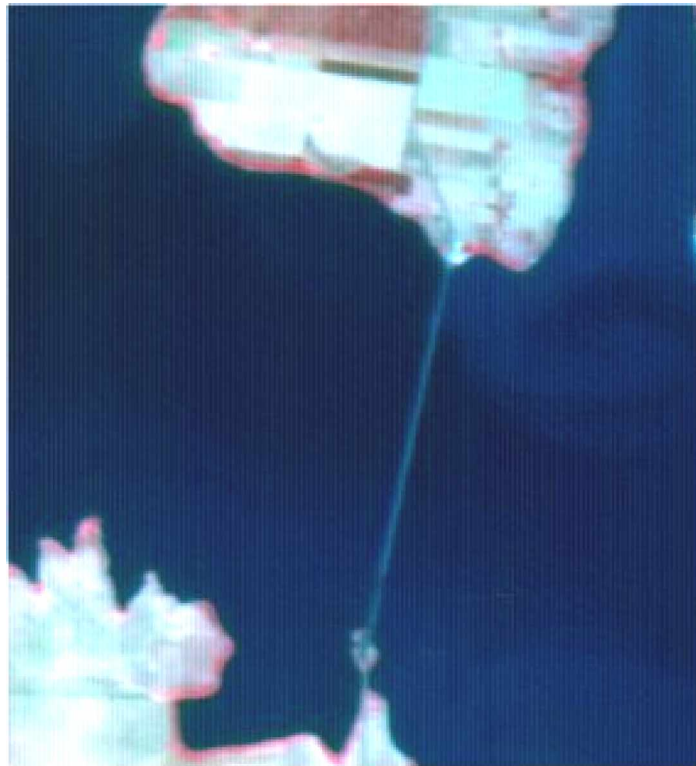Figure 1.4.5 - Pontchartrain bridge in Louisiana.

Figure 1.4.6 - Ilha Solteira (30/08/2004 and path/row:160-123).

MTF estimation Method

The spatial resolution estimation methodology is performed in the following steps (Kamel et al, 2004):

6. Identify targets with well-defined shape and size (bridges);
7. Model the bridge based on radiometric and geometric features of the bridge;
8. Simulate the Bridge model (Bridge axis identification);
9. Fit bridge model and bridge image;
10. Estimate the PSF and Calculate the effective spatial resolution.

The system point spread function is modeled as a 2D separable Gaussian function h_{σ_1,σ_2} centered at (u_1, u_2), that is,

$$h_{\sigma_1,\sigma_2}(x_1,x_2) = h_{\sigma_1}(x_1).h_{\sigma_2}(x_2)$$

$$h_{\sigma_1}(x_1) = \frac{1}{\sqrt{2\pi}\sigma_1} e^{-\frac{(x_1-u_1)^2}{2\sigma_1^2}}$$

$$h_{\sigma_2}(x_2) = \frac{1}{\sqrt{2\pi}\sigma_2} e^{-\frac{(x_2-u_2)^2}{2\sigma_2^2}}$$

The EIFOV value is related to the standard deviation σ so that EIFOV = 2.66σ , in both directions (across and along-track) . The PSF estimation in the along-track and across-track directions consists of finding σ_1 such that the real target image and simulated target image best fit under the root mean square criteria:

$$RMS = \left(\sum_{y \in G} \left[\left(f * h_\sigma \right) \left(T(y) \right) - g^j(y) \right]^2 \right)^{1/2}$$

Where:

σ = Standard deviation of the PSF model

g^j = real target image

f = target model

h_σ = sensor PSF

T_k = geometric transformation

$(f * h_\sigma), T_k$ = simulated target image.

Figure 1.4.7 shows the model fitting for band 3 (red: real target image and blue: simulated target image) and the third column of Table 1.4.3 shows the EIFOV values obtained.

The effective spatial resolution values for bands 1, 2, 3 and 4 are estimated using images of bridges Rio-Niteroi (along-track, bands 1-5), Ilha solteira (cross-track, bands 1 and 5) and Pontchartrain (cross-track, bands 2, 3 and 4) .
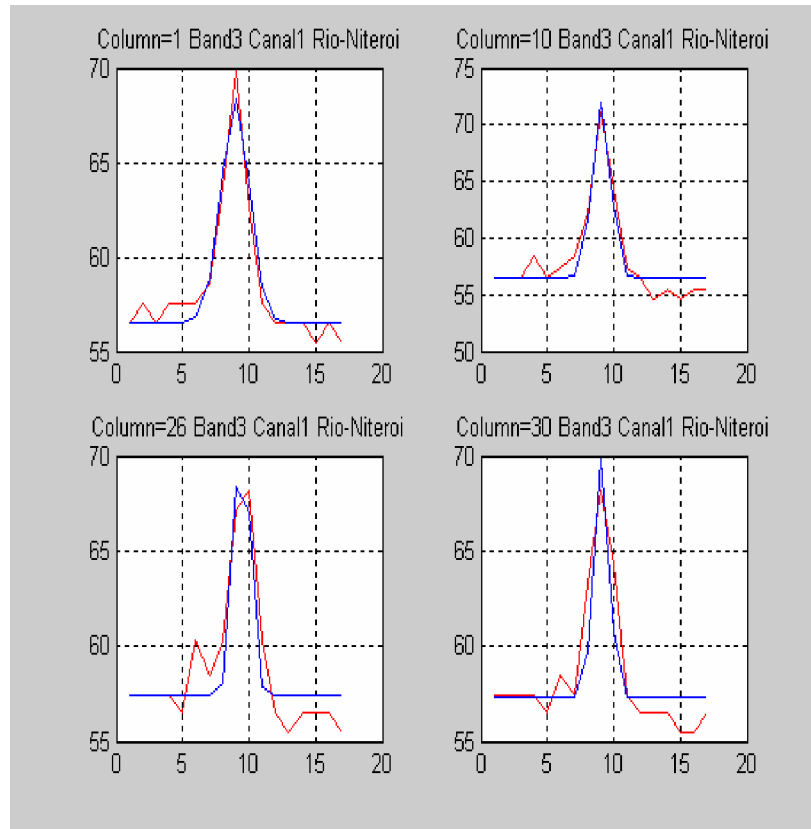
Figure 1.4.7 - Along-track fitting for band 3 (blue: simulated target and red: real target image).

Table 1.4.3 : EIFOV (m)

Bands	CBERS Bands (µm)	CBERS-2 (cross-track) laboratory	CBERS2(cross and along-track)	CBERS1(cross and along-track)	SPOT-3 (cross and along-track)	TM-5 (cross and along-track)
B1	0.45 – 0.52	30.4	61.0	66.0	- -	41.6
		-	36.0	36.0		45.4
B2	0.52 – 0.59	31	62.0	67.0	26.59	41.6
		-	39.0	37.0	28.1	45.4
B3	0.63 – 0.69	31	62.0	67.0	28.48	41.6
		-	47.0	40.0	29.95	45.4
B4	0.77 – 0.89	53	72.0	81.0	33.51	41.6
		-	45.0	64.0	30.93	45.4
B5	0.51-0.73	38	60.0	-		
		-	48.0	-		

In relation to the spatial resolution one concludes that:

1. In accord to the specifications the spatial resolution was degraded for all bands;
2. The resolution of CBERS2 CCD camera is a little better than CBERS1 CCD camera (band 4 has been improved)
3. the spatial resolution of CBERS-2 for all bands is worse than the SPOT-3 spatial resolution

The images in Figure 1.4.8 illustrate the low resolution of CBERS-2 in relation to SPOT-4 image and its improvement in relation to CBERS-1 quality. Figures 1.4.9-1.4.11 compare the corresponding spectral bands of CBERS1-CCD and CBERS2-CCD. One can observe that a significant improvement in band 4 of CBERS2-CCD.

(a)   (b)   (c)

Figure 1.4.8 — Visual quality comparison of (a) CBERS-1, (b) SPOT-4 and (c) CBERS-2 images.
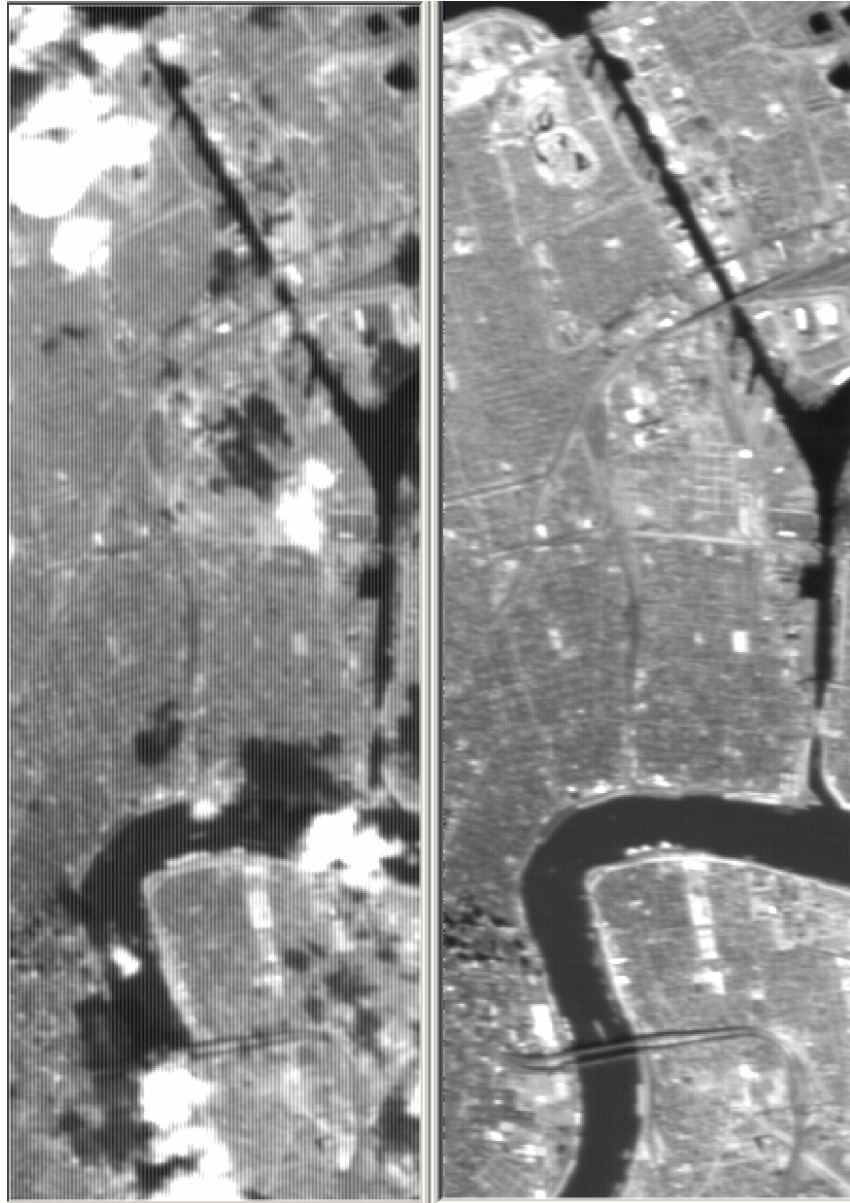
(a)   (b)

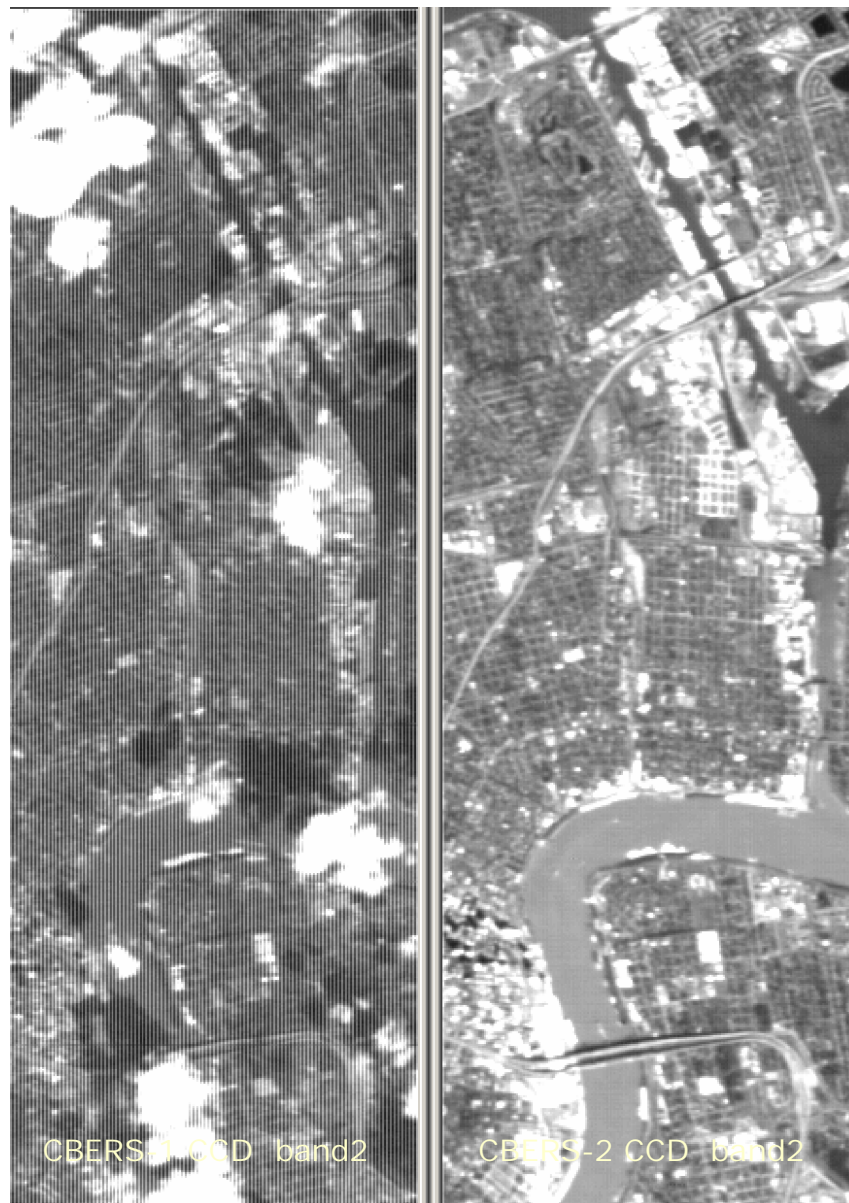Figure 1.4.9 — Visual quality comparison of (a) CBERS-1 and (b) CBERS-2 images for band 4.

(a)	(b)

Figure 1.4.10 – Comparing the visual quality of (a) CBERS-1 and (b) CBERS-2 images for band 3.

CBERS-1 CCD band2   CBERS-2 CCD band2

(a)   (b)

Figure 1.4.10 – Comparing the visual quality of (a) CBERS-1 and (b) CBERS-2 images for band 2.

1.5 Relative Calibration

The detector calibration process aims to correct the effects of the variability of the detector responses in the images. There are many ways to implement this process, which depends on the available calibration data. This section describes the calibration method implemented in the CBERS-2 Processing Station at INPE.

The CCD detector array arrangement consists of three arrays of 2048 detectors. During the telemetry data transmission, 6130 bytes are received in each line of the image and for each channel; 14 pixels in the third array are not received by the station. Within these data, 154 pixels in each array are superimposed and 8 pixels are dark. Figure 1.5.1 shows the detector arrangement for CBERS.
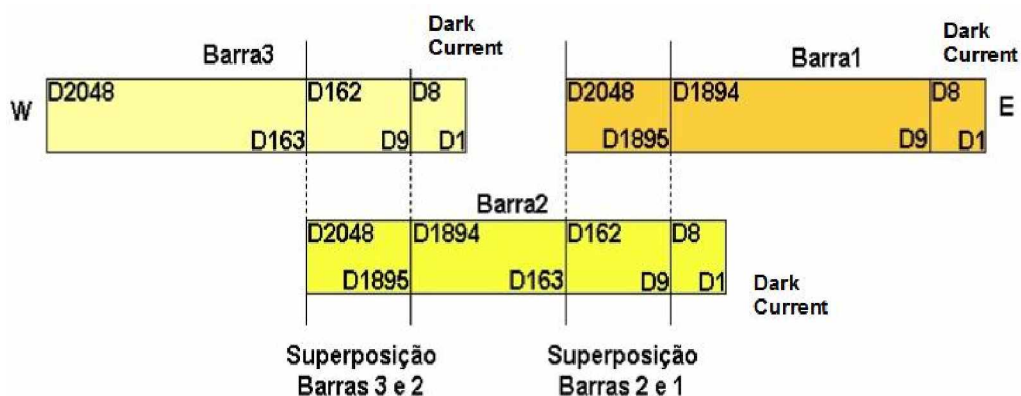

Figure 1.5.1 – CCD Detector Arrangement.

As one can see in Figure 1.5.1, there are two superimposed regions between the arrays (S12 and S23). Then, the final image contains 5798 pixels in a line. Any difference in calibration between these detectors, originating from factors such as power instability, will result in a noticeable difference between similar ground elements.

Each CCD detector of CBERS-2 is organized as shown in Figure 1.5.2, where the discharge of the CCD array is performed using two buffers, one for the odd-numbered detectors and other for the even-numbered detectors. These detector responses are then combined to produce the output data.
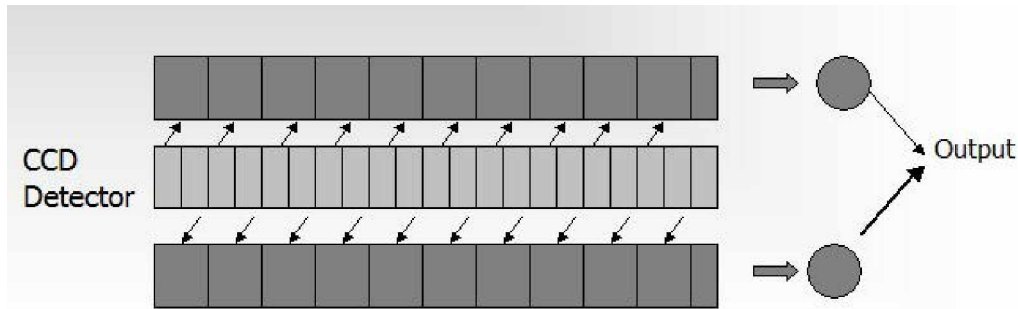
Figure 1.5.2 – Image Formation on the CBERS-2 CCD array.

Within each CBERS CCD array, there is an intra-detector variability, which needs to be detected and corrected. Besides, the radiation that reaches the superposition is divided between the arrays; the closer the border the lower radiation level.

The signal is generated into 2 channels: CCD-1 (B2, B3 e B4) and CCD-2 (B1, B3 and B5). Band 3 appears in both channels.

The detector response variation is caused by basically three factors:

§ A residual response for zero radiance, better known as "dark current" or "bias" or "offset", which , in practice, implies in a response different from zero when there is no illumination reaching the detector. This offset is unique for each detector;

§ A different gain for each detector which, in practice, results in different response for each detector for the same level of radiance;

§ The three detectors arrays have different average responses caused by a global gain difference among the arrays.

For CBERS-2 the experiments to obtain the calibration data were performed using the integrating sphere and the integrating semi-sphere. The integrating semi-sphere calibration data were obtained with the camera integrated with all subsystems in the integrating laboratory. Thus, these data look like better than the one of integrating sphere. (firstly, only 8 lines of integrating sphere calibration data were recorded; Escada asked CAST people to record more data). In accord to ETE (engineers at INPE) people the calibration data acquired from integrating semi-sphere are less uniform than one of integrating sphere.

For CBERS-2 CCD camera it is expected that the dark current values are lower, around 20 DN, as confirmed by CAST people (Zhang Yufeng, 03-07-16).

In order to illustrate, the graphics in the Figures 1.5.1-1.5.3 show the non-uniformity of CBERS-2 detector responses. The data were obtained using the integrating semi-

sphere. The first graphic (Figure 1.5.1) shows the three arrays responses while the second (Figure 1.5.2) and third graphics (Figure 1.5.3) show the first 100 pixels (including dark pixels) and the overlap region between the first and second array, respectively.
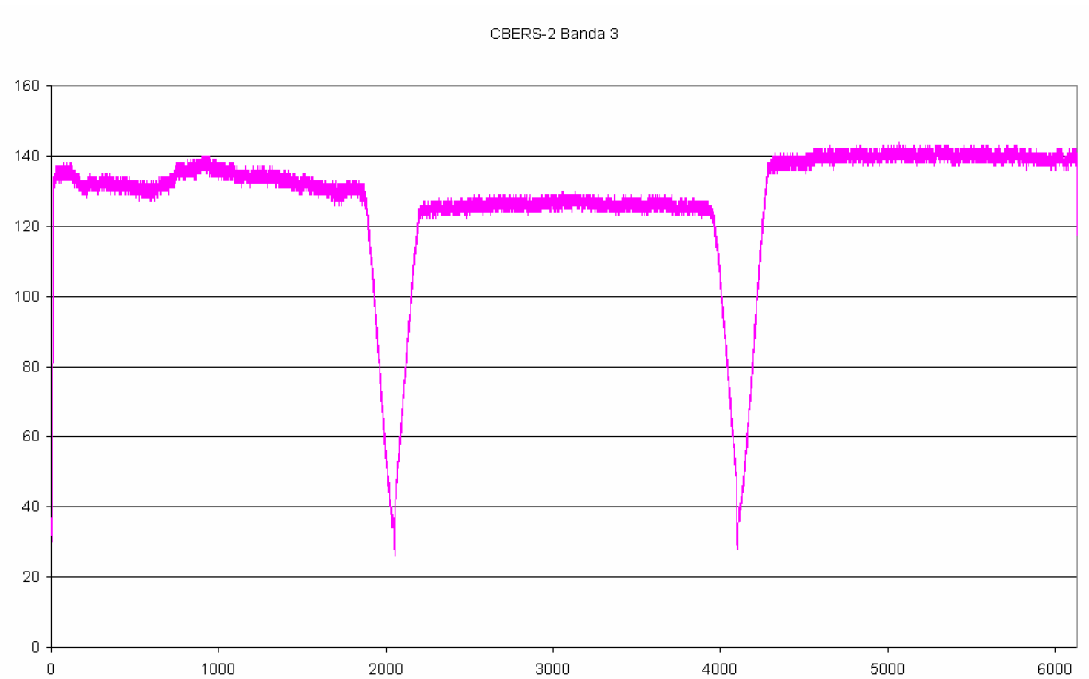

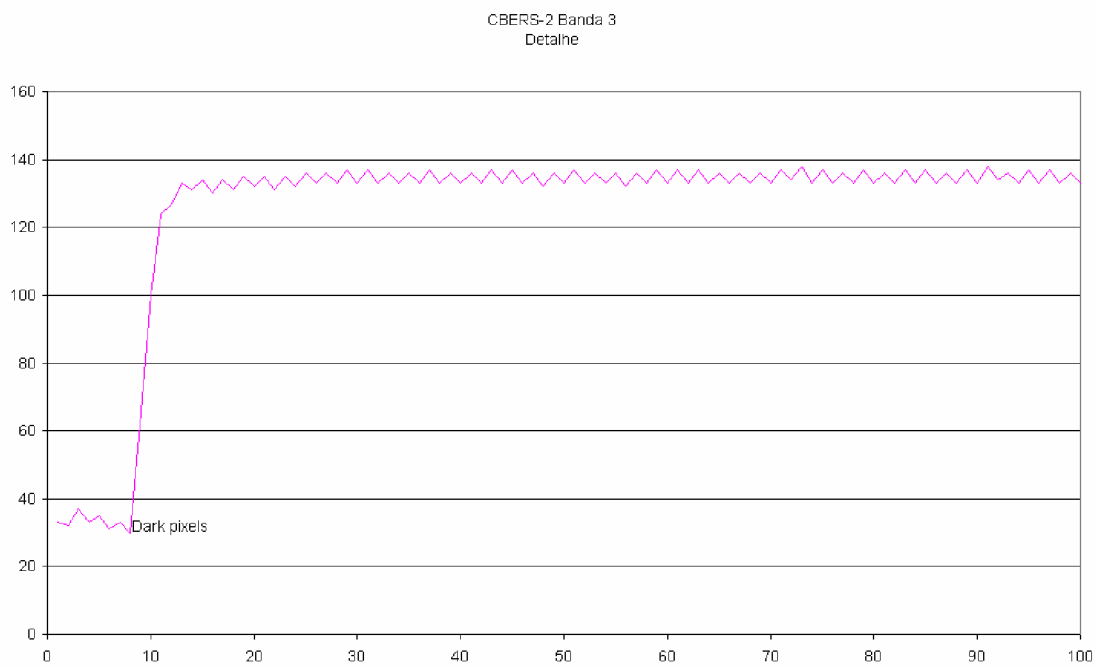Figure 1.5.1 – CBERS2-CCD: Responses of the detectors in the three arrays.

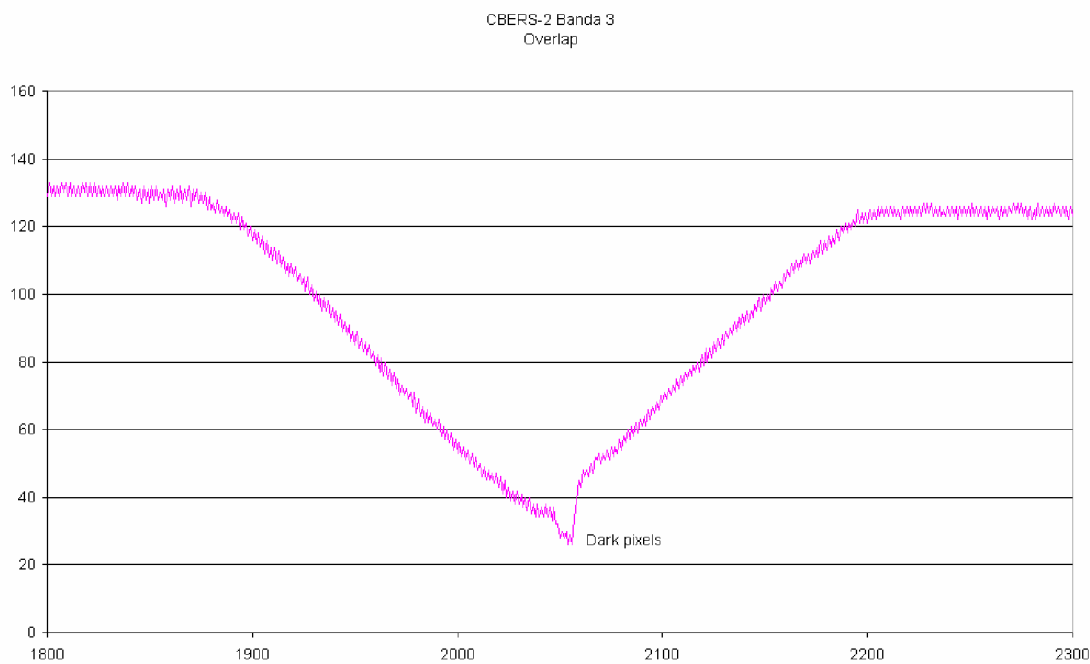Figure 1.5.2 – CBERS2-CCD: 100 detectors including the dark pixels.

Figure 1.5.3 - CBERS2-CCD: overlapping region between arrays 1 and 2.

In the calibration process the corrected pixel values are given by:

$$Y(b,a,p,g) = \frac{X(b,a,p,g) - O(b,a,p,g)}{G(b,a,p,g)} \qquad (1.5.1)$$

where :

X(b,a,p,g): DN value of the detector *p*, in the array *a* for the gain value *g* ,

Y(b,a,p,g): corrected pixel value for detector *p* of array *a* for the gain value *g*,

O(b,a,p,g): dark current offset for detector *p* of array *a* and for the gain value *g*,

G(b,a,p,g): gain coefficients for detector *p* of array *a* and for the gain value *g*.

All these parameters should be available for all spectral bands *b*. The coefficients of the equation (1.5.1) for all detectors, arrays and bands for each given instrument configuration form an "equalization coefficient set". CBERS2-CCD has 4 gains applied to each channel.

The traditional calibration method calculates the dark currents from an image with zero radiance level, take it off from each pixel in the image and calculate the gain values in order to equalize the sensor responses.

The CBERS-2 CCD calibration data were obtained for 13 radiance levels (given by the semi-sphere, (L=1,1,2,3 ...13)) and for the several configurations of the instrument gain. For each radiance level *L*,   400 lines of digital numbers were recorded for each band and array.

The calibration algorithm implemented in the CBERS-2 Processing Station at INPE has used the calibration data acquired by integration semi sphere. The data are saved in a file in an increasing order in relation to their intensity level, for each band (b=1, 2, 3a, 3b, 4 and 5) and for each array (a=1, 2 e 3). So, one has generated 18 synthetic images with 13 "bands" of different radiance levels, called "calibration image" (Figure 1.5.4) represented by $C_{(b,a)}$.

The 8 dark current pixels in each array are not used for any operation. Besides, only 380 lines of each "band" in the calibration image are used in the calibration parameters. The 10 first and 10 last lines are not considered in order to avoid noisy data.

The calibration function is a straight line (Figure 1.5.5) which can be defined by just two points, *P1= (X1,Y1)* and *P2=(X2,Y2)* :

$$Y = A.X + B \;,$$

where X and Y define the input and output DN values. The parameters *A* and *B* define de gain and offset of the calibration function.

Figure 1.5.4– Calibration image for banda 2, array 1, configuration gain=1 (pink color means saturated DN values).

It was observed that for some radiance levels and spectral bands the calibration data presented some anomalies (saturation and wrong variation of the DN values) as shown in Figure 1.5.5 and figures in the appendix. Thus, for each band it was chosen the best data to take into account in the calibration parameters calculation. The input DN value $X1$ for point $P1$ is obtained from the calibration data in the radiance level zero ($L=0$). The other has been selected (L_r) as one of the radiance levels in which the calibration data are the good. The third column of Table 1.5.1 shows the selected radiance level for each band.

The values X1 and X2 are defined by the average value of each detector d in band b, array a and radiance level l:

$$M(b,a,p,l) = \frac{1}{380} \sum_{i=10}^{389} c_i(b,a,p,l).$$
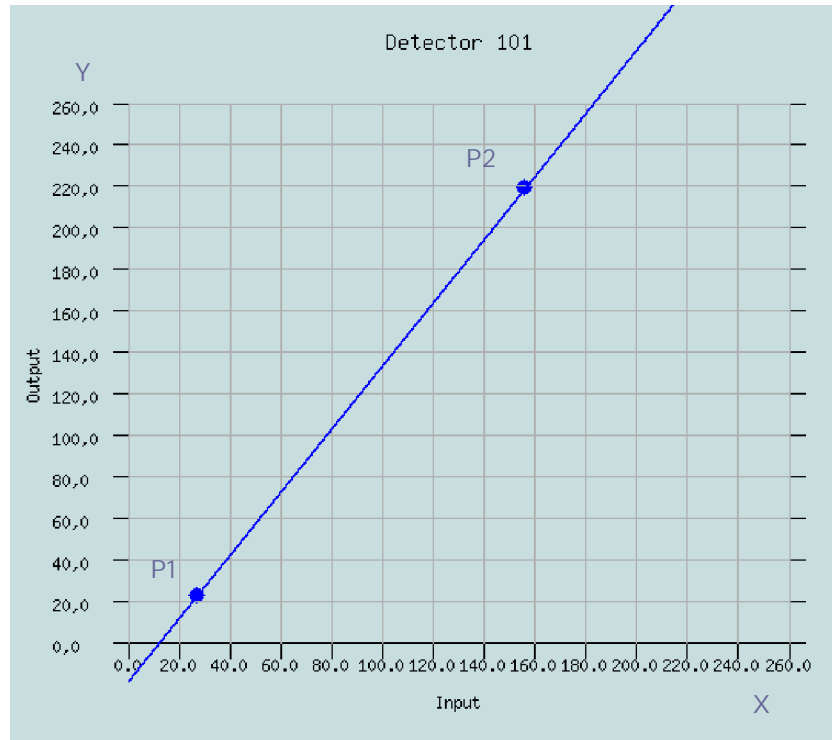
Therefore,

$$X_1 = M(b,a,p,0)$$

$$X_2 = M(b,a,p,L_r).$$

Figure 1.5.5– Calibration function for detector 101.

The output DN value for *P1* is defined as *Y1=0*, that is *P1=(M(b,a,p,0),0)*. Thus, *P1* define the zero-crossing in the coordinate X. The output DN values (Y2) for all bands are shown in the forth column of Table 1.5.1.

Table 1.5.1: Radiance levels and output DN used in the calibration calculation.

Band	Array	Radiance level	Output DN
	1	8	64
B1	2	8	64
	3	8	64
	1	8	208
B2	2	8	208
	3	8	208
	1	8	240
B3	2	8	240
	3	8	240
	1	4	215
B4	2	4	215
	3	4	215
	1	8	218
B5	2	8	218
	3	8	218

Each array in each band is corrected using the calibration function defined as mentioned above. The pixel values in the overlap regions (154 pixels) between arrays 1 and 2 (S1) and 2 and 3 (S2) (Figure 1.5.6) are weighted by the distance (inversely proportional) and then added up: the lower DN values the higher their weights.

S12:

$$DN1(i) = DN(i)*((155-j)/155) + DN(i+154)*(j)/155 \quad (i=1887\text{-}2040; j=1,...,154)$$

S23:

$$DN2(i) = DN(i)*((155-j)/155) + DN(i+154)*(j)/155 \quad (i=3935\text{-}4088; j=1,...,154)$$
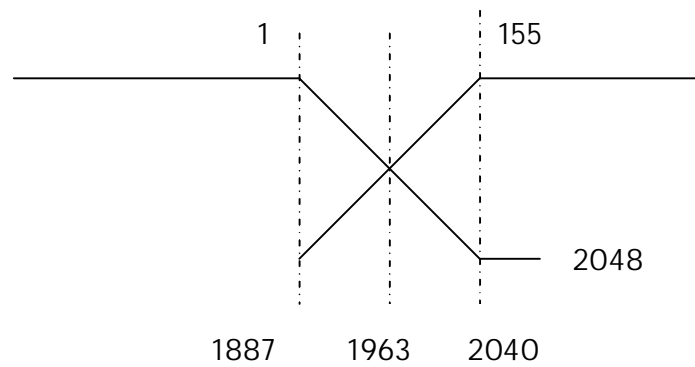
Figure 1.5.6 - Overlap region S1 (154 pixels).

Figure 1.5.7 shows the original calibration data (band 4, array 1, L=4) and the data after calibration.
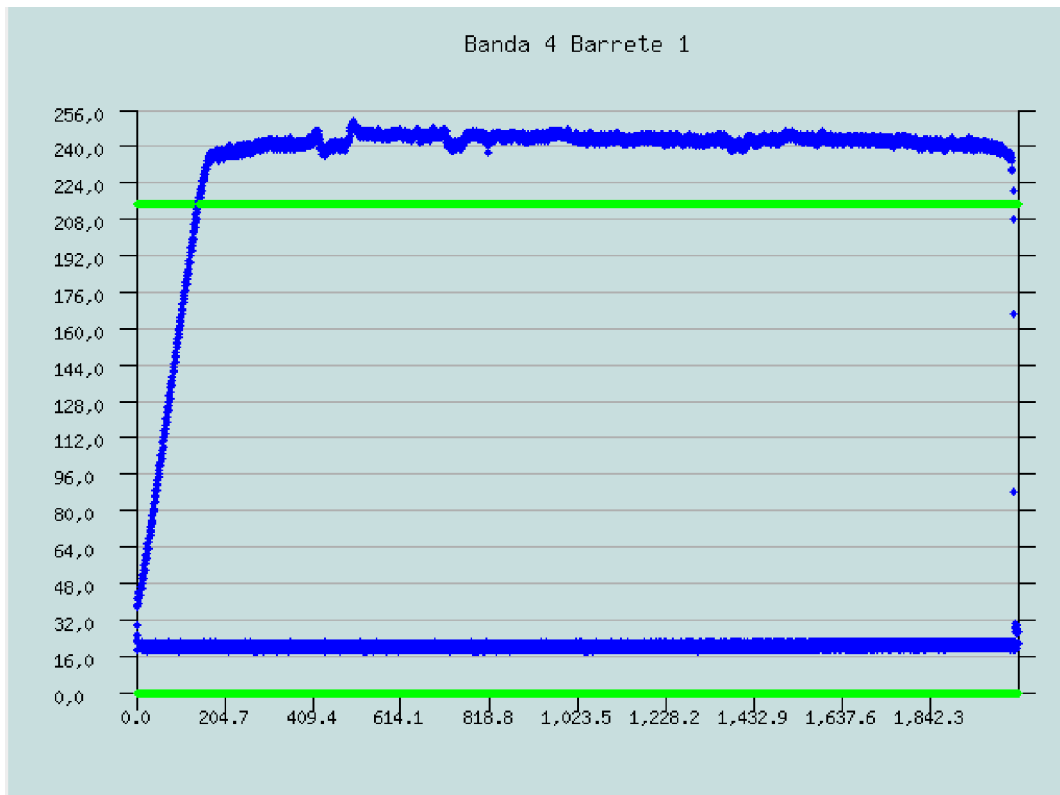
Figure 1.5.7 – Original (blue) and corrected (green) calibration data. The curves in the bottom are the gain (green, about 1.0 DN) and offset (blue, about 20 DN).

Some data acquired by detectors are out of specification. From analysis of the raw data, the processing system identifies the non-conform detectors and generates a list of what is known as defective detectors.

The defective detector processing is done by interpolation of data. This interpolation is parameterized according to the parameter *maxnc*, which declares the maximum number of detective columns to be interpolated. The radiometry of the defective detectors is not used. The defective detector value is replaced by a linear interpolation on the nearest valid columns surrounding the invalid column.

If the number of adjacent defective detectors is higher than *maxnc*, their radiometry is replaced by 0.

1.6 In-flight Absolute Calibration

The success of any remote sensing project is directly related to the knowledge of both spectral and radiometric characteristics of the sensor from which the data will be available. A good example is the Thematic Mapper (TM) sensor of the Landsat satellites program, whose dynamic radiometric characteristics have been updated since some days after launch. The easy access of this information has allowed the conversion of the Digital Numbers (DN) of the TM images into physical data like radiance or reflectance, which can be related to the biophysical and geophysical parameters.

Since the CBERS-2 has been launched and the first CCD images have been available in INPE´s home page, users have been asking information about how to convert the DN values into physical data. There are many scientific tasks that depend on this information.

This section describes the procedure performed by INPE to calculate the in-flight absolute calibration coefficients for CCD sensor considering the reflectance-based method.

The Calibration sites

A calibration site must present some desired characteristics (Scott et al,1996) :

1. A bright site (reflectance greater than 0.3) to reduce the impact of errors in the atmospheric correction;

2. Altitude > 1km to reduce aerosol loading and the errors associated with the predicting their effects;

3. Spatial uniform to a level of 2% over at least a 2 x 2km area to minimize misregistration effects;

4. Minimal seasonal variations in surface reflectance;

5. An arid region to reduce the probability of clouds and reflectance variations from changing surface moisture;

6. Nearly isotropic with flat topography to simplify bi-directional reflectance characterization and reduce uncertainty from surface bi-directional effects;

7. Spectrally flat surface reflectance to simplify band-to-band comparisons within sensors and across sensors and

8. Accessibility.

Considering the geomorphology of the Brazilian territory, there are no surfaces that have all these eight desired characteristics. However, some calibration sites in the west part of the State of Bahia were identified that meet the following characteristics:

1. The region presents low cloud cover indices during winter time at the satellite over pass;

2. The altitude is about 850 m over the sea level;

3. Sand is the dominant soil (relative high reflectance);

4. During the winter time, large areas of economical crops are prepared to plant and they present enough dimensions for CBERS-2 sensors calibration proposes;

5. The agricultural schedule performed every year makes possible to find a specific calibration site with the same characteristics at a specific time of year;

6. The reference surfaces presents enough isotropy during the calibration time;

7. The spectral/spatial uniform is about 6-8%;

8. The region is one of the most arid region of the Brazilian territory;

9. The reference surfaces are located in the farms. Therefore, the access is very easy because there are a lot of roads.

Figure 1.6.1 shows the localization of the calibration region in the Brazilian territory including the average cloud cover indices for June 2003. The red ring indicates the interest region.
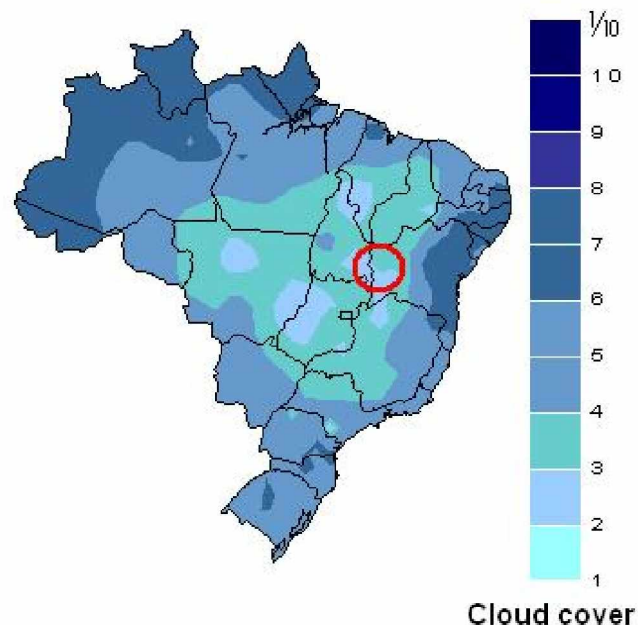

Cloud cover

Figure 1.6.1 – Localization of calibration sites in Brazil.

Two field campaigns to characterize some potential reference surfaces and to collect radiometric were performed. In both campaigns it was considered the CBERS-2 path/row 156/113, 06/25/2004 and 08/16/2004.

The first campaign was carried out in June 2004, in which four reference surfaces were evaluated. The second one was performed in August when another four potential surfaces were also evaluated. Figure 1.6.2 shows a color composition (B2 (G), B3 (B) and B4 (R)) of a CCD image acquired on 06/25/2004. The reference surfaces are indicated by yellow circles.

Figure 1.6.2 - Reference surfaces indicated by yellow circles.

Yellow rings indicate the crop fields that were selected as a reference surface to be radiometrically characterized. Only 2 out of 8 surfaces were used in the CCD/CBERS-2

absolute calibration process. Therefore, these two reference surfaces will be described. Surface 8 located in the extreme east of the image was not utilized due to CBERS-2 orbit deviation.

The image evaluation considered two different approaches including the spectral homogeneity and the isotropy. The first one was based on radiometric measurements from the surface which was carried out using the ASD FieldSpec spectroradiometer running from 350 to 2500nm. In order to evaluate the spectral homogeneity of the surfaces the measurements started at 9:00 am and finished at 11:00 am, close to the satellite over pass time The same radiometric measurements to evaluate the surfaces isotropy were carried out from 8:00 am until 12:00 at every 30 minutes, approximately. The idea here was to identify any tendency in the bidirectional reflectance factors since the illumination geometry had been changed. Figure 1.6.3 shows a picture to illustrate how these measurements were performed in the surface indicated as 1 in Figure 1.6.2.

Figure 1.6.3 – Radiometric measurements performed with ASD FieldSpec spectro-radiometer in the reference surface 1.

The surface 1 (Figure 1.6.2) was effectively utilized in the first calibration campaign performed in June 2004. It is composed by a silted soil (darker than the others). It presents an apparent spectral homogeneity despite being a very large surface. In terms of spectral homogeneity this surface presented relatively

high Variation Coefficients (VC) in relation to the other surfaces (from 8% to 11.5%). Figure 1.6.4 shows the curve of the average Reflectance Factor and its Standard Deviation (+ and -). Figure 1.6.5 shows the reflectance factor curves calculated for different time of collecting data in the surface 1.
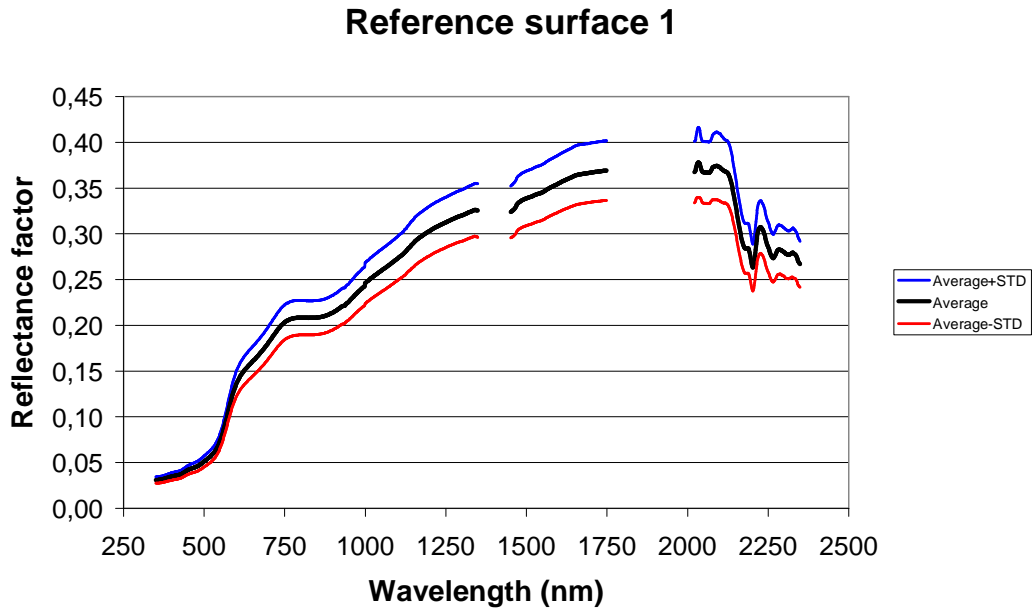
Reference surface 1

Figure 1.6.4 — Average reflectance factor and standard deviation for surface 1.

Surface 1- Isotropy
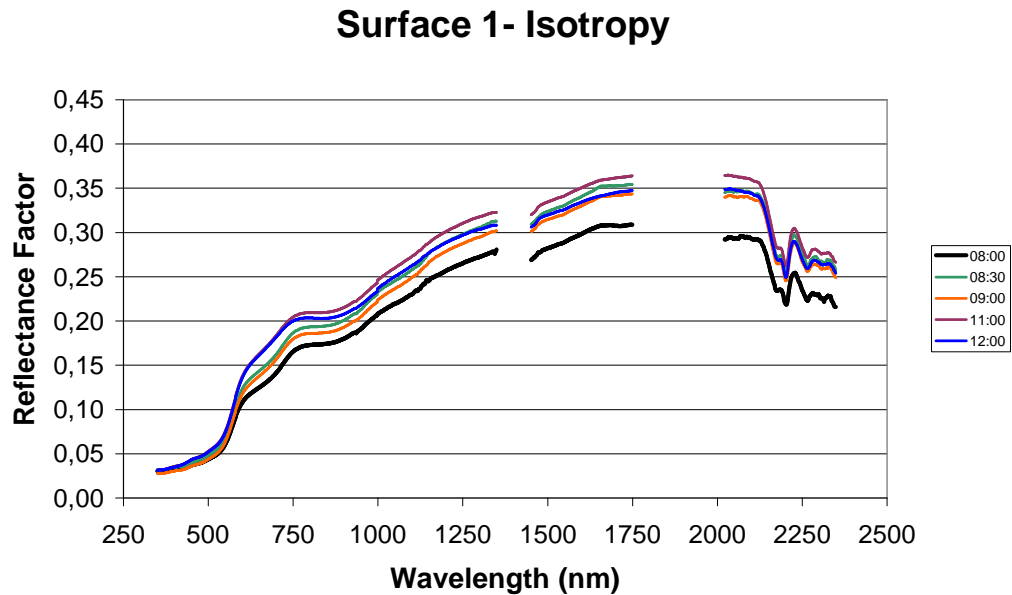
Figure 1.6.5 Reflectance factor curves calculated for different time of collecting data in the surface 1.

One can notice that there is no a specific tendency in the curves according the different time of collecting data which indicates that the surface is enough isotropic for calibration purpose.

The reference surface 2 (Figure 1.6.2) used in the second calibration campaign (August of 2004) was spectrally characterized twice (June and August) because it was observed differences in the soil granulation. In June the characterization was carried out in a region where the soil particles were bigger than those ones in the region characterized in August. The surface is composed by a sandy soil (brighter than the others) as illustrated in Figure 1.6.6.

big particles

small particles

Figure 1.6.6 – Reference surface 2 composed by a sandy soil.

In spite of being smaller than the surface 1 the surface 2 presented lower VC values than the surface 1 (7 to 10% in June and 8 to 10% in August), considering all the ASD FieldSpec spectral range. Figure 1.6.7 shows the average reflectance factor curve and its standard deviation for the data collected in June (bigger) and August (smaller).
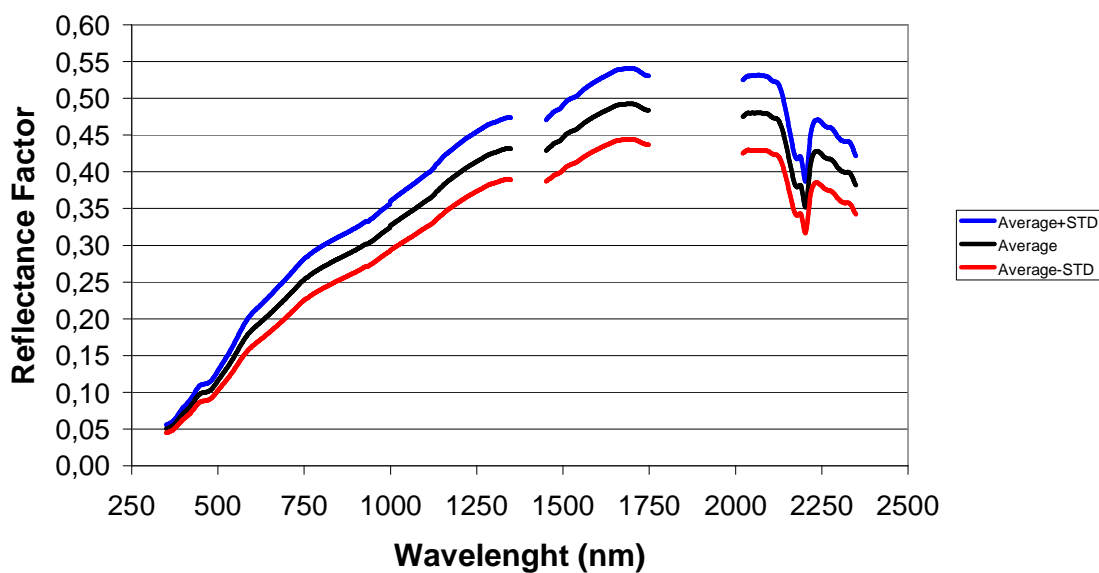
Reference Surface 2 Smaller

Figure 1.6.7 – Average reflectance factor and the standard deviation for surface 2.

One can be noticed that there are no significant differences between the data analyzed in the two field campaigns. Figure 1.6.8 shows the reflectance factor curves calculated for different time in the surface 2 for isotropy evaluation proposes.

In June, one was verified that the reflectance factor has dropped as well as the solar elevation has increased. The great difference between the reflectance factors obtained at 07:40 am can be explained by the isotropic limitations of the reference panel utilized during the radiometric measurements. It is not isotropic for low solar elevation angles.

Calibration data

As mentioned above, two calibration campaigns were carried out (June and August). The radiometric data were collected around a specific point arbitrarily identified in the reference surface. This point was adopted as a center of an imaginary cross and 40 radiometric measurements were performed (10 per each cross branch). An arithmetic average among these 40 measurements was calculated and assumed as the pixel reflectance in the CCD images.
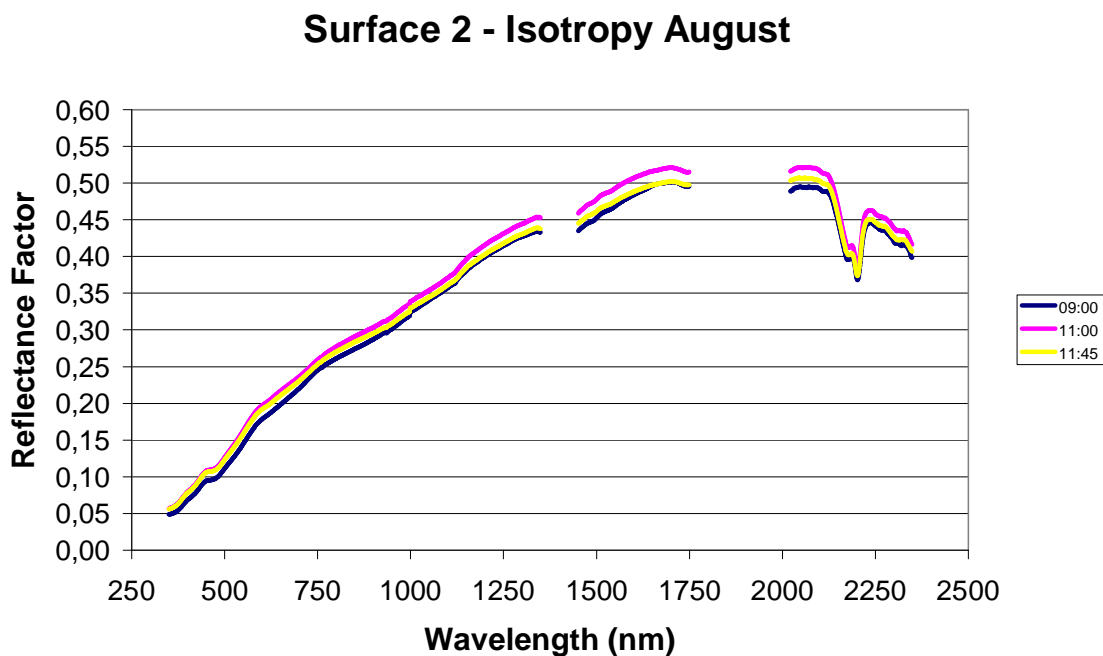
Surface 2 - Isotropy June

Surface 2 - Isotropy August
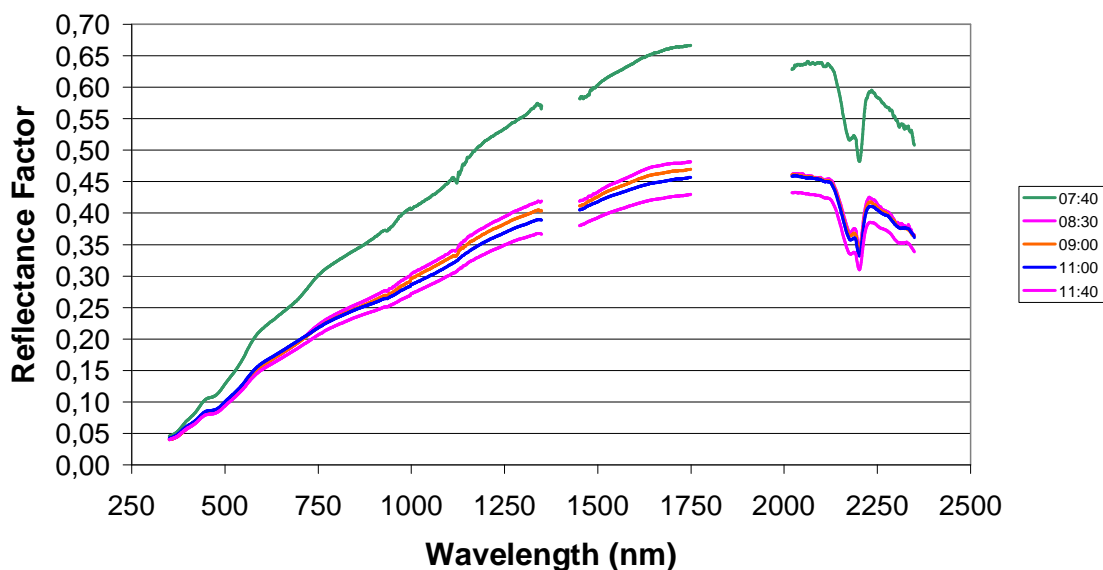
Figure 8 — Reflectance factor curves for different time of collecting data in surface 2 in June and August.

VC values obtained from the 40 radiometric measurements were about 8% to 9% and 6% to 8% for the surfaces 1 (June) and 2 (August), respectively.

Table 1.6.1 shows the reflectance factors obtained from surface 1 for each spectral band of CBERS-2 sensors (WFI, CCD and IRMSS). The central coordinates are -46º 05′ 16.8 and -11º 55′ 37.0

Table 1.6.1 — Reflectance factors for CBERS-2 sensors (surface 1, June).

	WFI		CCD		IRMSS
B1	0.1610	B1	0.0460	B1-PAN	0.1823
B2	0.2005	B2	0.0812	B2	0.3382
		B3	0.1610	B3	0.2834
		B4	0.2005		

B5-PAN	0.1305

The same procedure was carried out for the surface 2 (August) and the results are shown in Table 1.6.2. The central coordinates are -46º 00′ 23.5 and -12º 06′ 44.6.

Table 1.6.2 – Reflectance factors for CBERS-2 sensors (surface 2, August).

WFI		CCD		IRMSS	
B1	0.2262	B1	0.1182	B1-PAN	0.2758
B2	0.2977	B2	0.1679	B2	0.5099
		B3	0.2262	B3	0.4509
		B4	0.2977		
		B5-PAN	0.2040		

The reflectance factors were considered as the basis for the apparent radiance calculation through the application of the 5S atmospheric correction model. This procedure will be described later.

Atmospheric correction

The atmospheric measurements were performed using a manual sunphotometer CE317/ CIMEL running in the following spectral bands: B1: 1010 to 1030 nm; B2: 860 to 880 nm; B3: 660 to 680 nm; B4: 430 to 450 nm and B5: 926 to 946 nm.

The atmospheric characterization was based on measurements of direct solar radiation whose output V can be written as:

$$V = V_0 \times D_S \times t_g \times e^{-\tau \times m} \tag{1}$$

where V: sunphotometer output;
V_O: calibration coefficient;
D_S: Sun-Earth distance factor, given by Equation 2:

$$D_S = \frac{1}{1 - 0.01673 \times \cos[0.9856 \times (J - 4)]} \tag{2}$$

where J: is the day of year;
t_g: gaseous transmittance ($\cong 1$ in the spectral regions of the CE317/Cimel bands);

τ: total optical depth of atmosphere, calculated by Equation 3:

$$\tau = \tau_{RAYLEIGH} + \tau_{AEROSOLS} \tag{3}$$

where $\tau_{AEROSOLS}$ is the optical depth due to aerosol scattering and $\tau_{RAYLEIGH}$ is the optical depth due to Rayleigh scattering given by:

$$\tau_{RAYLEIGH} = \frac{(84.35 \times \lambda^{-4} - 1.255 \times \lambda^{-5} + 1.4 \times \lambda^{-6}) \times 10^{-4} \times P}{1013.25} \tag{4}$$

where P is the local atmospheric pressure in hPa and λ (in µm) is the wavelength and m: air mass number, given by :

$$m = \left[\frac{1}{\cos\theta_S + 0.15 \times (93.885 - \theta_S)^{-1.253}} \right] \times \frac{P}{1013.25} \tag{5}$$

where P is the atmospheric pressure in hPa and θ_S (in degrees) is the solar zenith angle.

Applying the natural logarithm on the both sides of Equation 1, it can be rewritten as follows:

$$\ln\left[\frac{V}{D_S \times t_g} \right] = \ln V_0 - \tau \times m \tag{6}$$

The plot of In $[V / (D_S \times t_g)]$ versus m, for several solar zenith angles and an assumed stable atmosphere, gives the calibration coefficient V_O (= $e^{intercept}$) and the total optical depth τ (= - *slope*). This method, known as Langley Method, was used to characterize the atmosphere, based on measurements performed on August 17th according to the schedule presented in Table 1.6.3. The mean atmospheric pressure P during that day was 922.5 hPa.

Table 1.63 – Measurement schedule.

Date	D_S	N	First Measurement			Last Measurement		
			Time	θ_S	m	Time	θ_S	m
Aug 17th	0.9751	49	6:34h	86.57	12.617	12:11h	26.00	1.012

The calibration coefficient V_O and the total optical depth τ for each band calculated by the Langley Method are shown in Table 4.

Table 1.6.4 – Sunphotometer Calibration.

Cimel Band	$\lambda_{CENTRAL}$ (µm)	R^2	V_O	τ	$\tau_{RAYLEIGH}$	$\tau_{AEROSOLS}$
1	1.020	0.9612	6460.5738	0.0350	0.0071	0.02791
2	0.870	0.9628	13441.4594	0.0369	0.0135	0.0234
3	0.670	0.9876	15459.9252	0.0741	0.0387	0.0354

4	0.440	0.9986	4250.22028	0.2668	0.2155	0.0513

According to the Angström's turdibity formula, the spectral variation of aerosol optical depth $\tau_{AEROSOLS}(\lambda)$ can be written as:

$$\tau_{AEROSOLS}(\lambda) = \beta \times \lambda^{-\alpha} = 0.02475 \times \lambda^{-0.8562}, \text{ with } R^2 \cong 0.9 \tag{7}$$

where α is related to the average aerosol size distribution and β is the Angström turbidity coefficient that is proportional to the quantity of aerosols and related to the horizontal visibility in km (*VIS*) according to the following equation:

$$\beta = 0.613 \times e^{\frac{-VIS}{15}} \tag{8}$$

Consideing that β = 0.022475 (Equation 7) then VIS $\cong$ 48km that corresponds to a clear atmosphere at sea level.

The spectral variation of total optical depth $\tau(\lambda)$ can be written as follows:

$$\tau(\lambda) = 0.00623 \times e^{\frac{1651.527}{\lambda}}, \tag{9}$$

with R^2=0.9978.

The Cimel band centered on 936 nm was employed to estimate the water vapor contents (*UW*) since there is an important absorption band due to water vapor in this spectral region. The gaseous transmittance t_g was not approximate by 1, as the other bands, but estimated using the following expression:

$$t_g = e^{-0.6767 \times UW^{0.5093} \times m^{0.5175}},$$

where *m* is the air mass number. $\tag{10}$

The equation of the Langley Method is rewritten as:

$$\ln\left[\frac{V \times e^{-\tau \times m}}{D_S}\right] = \ln V_0 - UW^{0.5093} \times (0.6767 \times m^{0.5175}). \tag{11}$$

Using the data acquired August 17th and knowing that τ (0.936 nm) = 0.03391 (Equation 9), the Langley plot gives: V_O = 18724.70, *UW* = 2.403 g/cm², R^2 = 0.9978 for 49 experimental points.

Since the sunphotometer was calibrated, the solar direct irradiance was also measured at the same time as radiometric measurements were performed for CCD calibration

(June and August). The data utilized for 5S atmospheric correction model for these specific campaigns are presented on Table 1.6.5.

Table 1.6.5 – Input data for atmospheric correction by **5S**.

Campaigns	$\tau\,aer$ (0.55 nm)	UW (g/cm^2)	O_3
06/25/2004	0.03708	2.91342	0.253
08/16/2004	0.02693	2.44000	0.248

The 5S results are presented in Tables 1.6.6 e 1.6.7 for both field campaigns.

Table 1.6.6 – 5S results for calibration campaign in June.

June	L_{apa} (W.m^{-2}.sr^{-1}.µm^{-1})	Eo (W.m^{-2}.µm^{-1})
CCD-1	41.5385	1934.03
CCD-2	37.7661	1787,10
CCD-3	51.8571	1587.97
CCD-4	41.4560	1069.21
CCD-pan	47.8991	1664.33

Table 1.6.7 – 5S results for calibration campaign in August.

August	L_{apa} (W.m^{-2}.sr^{-1}.µm^{-1})	Eo (W.m^{-2}.µm^{-1})
CCD-1	70.3385	1934.03
CCD-2	70.9677	1787,10
CCD-3	77.1111	1587.97
CCD-4	66.7680	1069.21
CCD-pan	76.1788	1664.33

Obs.: L_{apa} is the apparent radiance (top of the atmosphere) and Eo is the solar irradiance in the top of the atmosphere.

Comparing the coefficients calculated here with those determined in pre-launch conditions, it seems that those calculated in August (using a brighter reference surface) are closer to the pre-launch ones.

The conversion of DN in L_{apa} is done by the equation:

$$L_{apa} \ (W.m^{-2}.sr^{-1}.\mu m^{-1}) = DNn/CCn \qquad (12)$$

where:

L_{apa}= apparent radiance;

DNn= digital number extracted from the image in band n (n=1,2,3,4,pan);

CCn= calibration coefficient for band n (n=1,2,3,4,pan).

That L_{apa} can be converted in apparent reflectance by the following equation:

$$\rho_{apa} = (3,1423*(DNn/CCn)*D**2)/(Eon*cos(zen)) \qquad (13)$$

where:

D = Earth-Sun distance in astronomic units;

Eon = Solar Irradiance in the top of the atmosphere in band n (n=1,2,3,4,pan);

$cos(zen)$= cosine of the solar zenith angle at the image acquisition time.

Preliminary evaluation

The pre-launch and in-flight calibration coefficients were applied in images from June and August in order to evaluate if a specific object could be spectrally properly characterized, at least in the top of atmosphere terms. A non-vegetated surface located near the surface 2 was chosen at first and the apparent reflectances determined by both pre and in-flight calibration coefficients were extracted from CCD images (from August) and compared with the surface reflectances (from the radiometric measurements performed in the field). Figure 1.6.9 shows the reflectance factors curves.
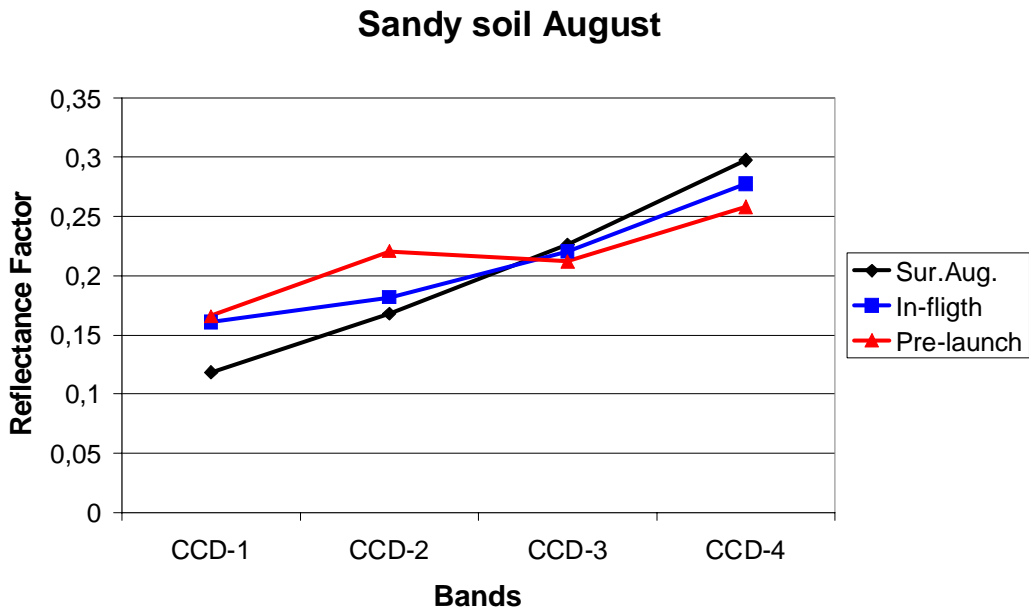
Sandy soil August

Figure 1.6.9 — Reflectance factor curves for surface, in-flight and pre-launch conditions.

The differences between the curves are expected since in the visible region the atmosphere adds energy in the radiance measured by the sensor, while in the near infrared region it reduces the radiance in the entrance of the pupil by the absorption phenomena. The results obtained by applying the in-flight calibration coefficients seem much better than those obtained by the pre-launch ones.

A vegetated pixel was also chosen to do a similar evaluation and the results are presented in Figure 1.6.10 but without data from the field.

Pre-launch CC Vegetation

In-fligth CC Vegetation
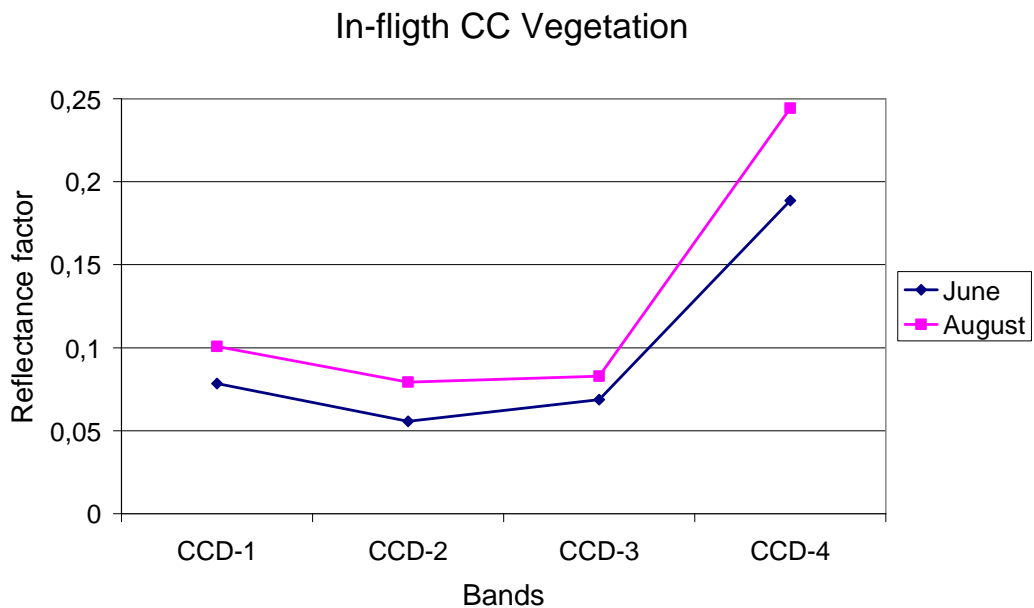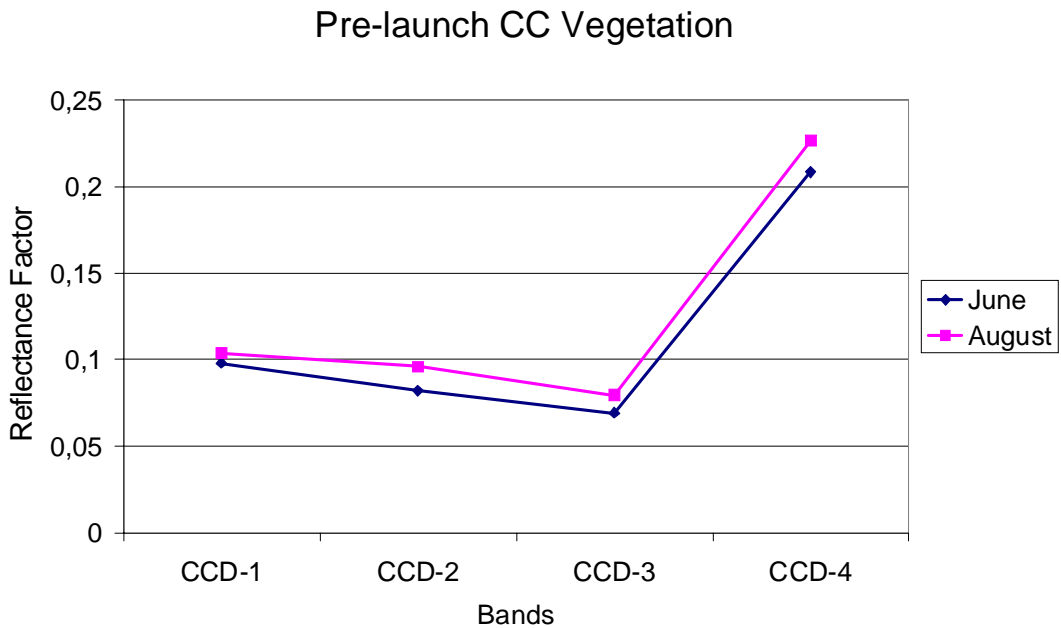
Figure 1.6.10 – Reflectance factor for a vegetated pixel using pre and in-flight calibration coefficients.

Finally, the calibration coefficients obtained by two experiments (June and in August) were tested to evaluate the performance of both set of coefficients. In this case, the pre-launch calibration coefficients applied in both images (June and August) look like to represent properly the target spectral characteristics. The main difference between pre-launch and in-flight coefficients determined in

August has been observed in the spectral band B2 (CCD). Those coefficients determined in June don't result good target spectral characterization.

2. WFI camera

The WFI has a ground swath of 890 km which provides a synoptic view with spatial resolution of 260m. The Earth surface is completely covered in about 5 days. It has two bands 0.63 - 0.69 µm (red) and 0.77 - 0.89 µm (infrared), which are also present in the CCD camera to allow complementing the data of the two types of remote sensing images.

One was observed in some WFI images (vegetation) radiometric differences in their left side (Figure 2.1). Probably, this effect is due to the Bidirectional Reflectance Function (BRF), which describes the directional dependence of the radiation reflection of vegetation.

Figure 2.2 shows the image (Figure 2.1) after applying a weighting function (lighter regions are weighted with lower coefficients than the darker regions) to correct the BRF effect.
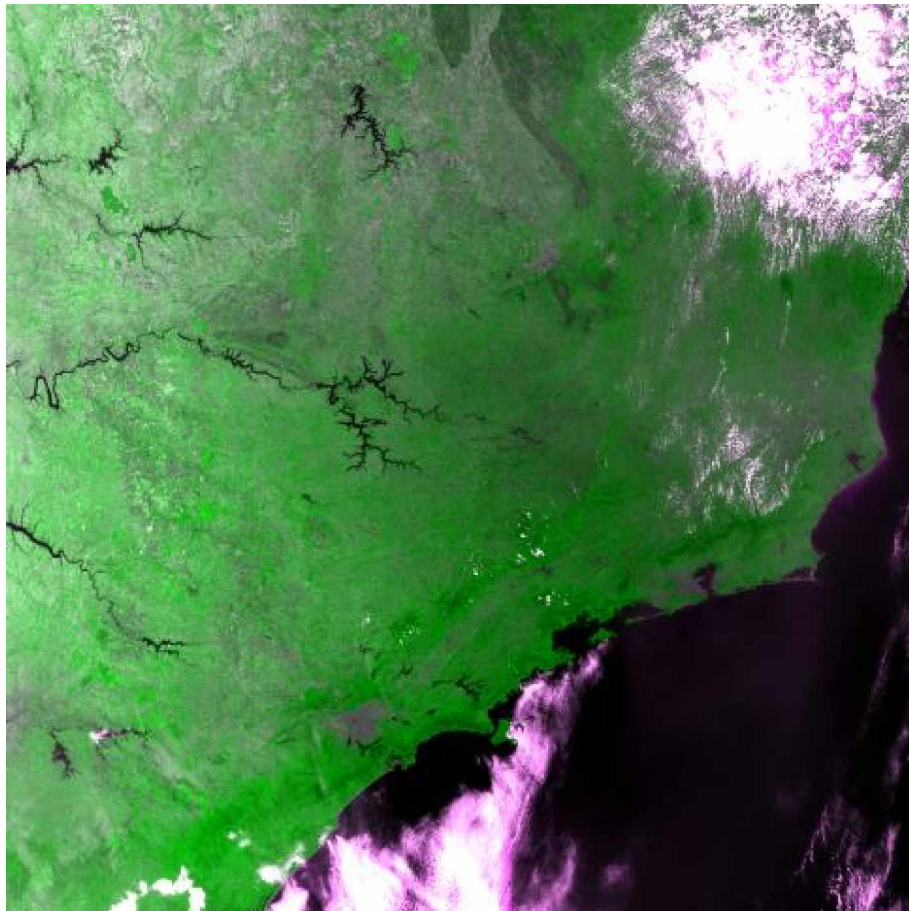
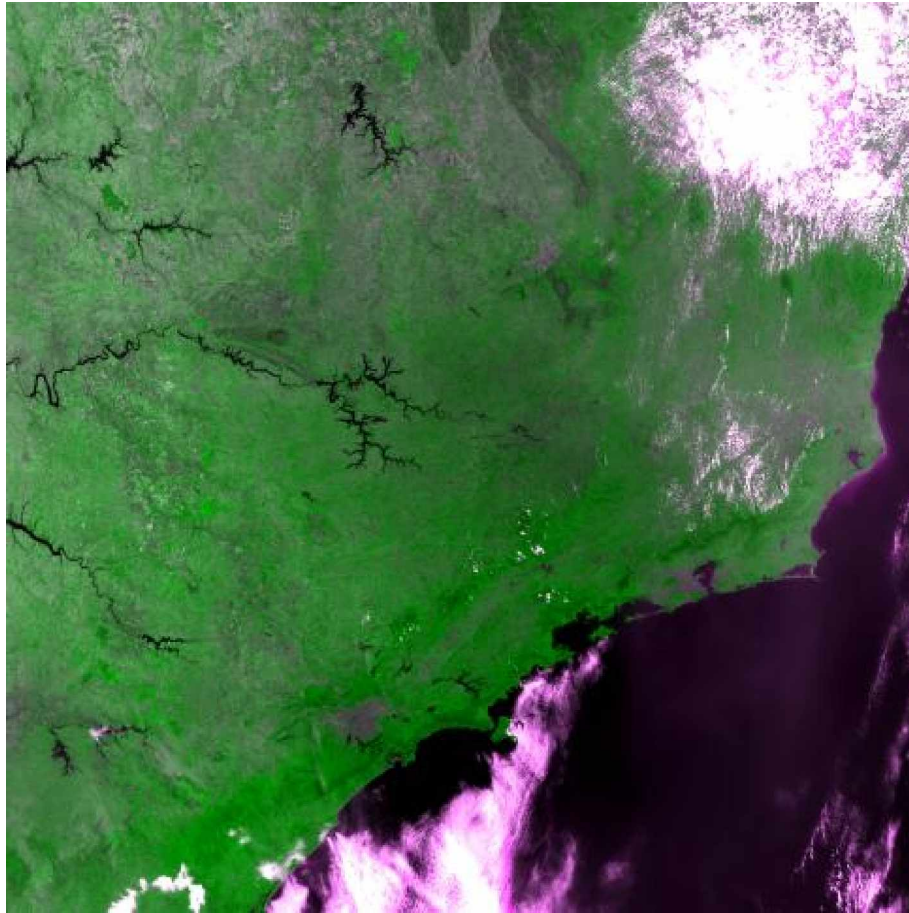Figure 2.1 — Brightness difference in the left side of the image.

Figure 2.2 – Image after brightness difference correction.

Relative calibration

Relative and absolute calibration coefficients were obtained in laboratory before satellite launching by engineering people at INPE.

The calibrated data Y is obtained by applying the following equation:

$$Y(n,b) \;=\; \frac{X(n,b,m) \;-\; C(n,b,m)}{\gamma(b,m) \quad g(n,b)} \; , \tag{3.1}$$

where,

X(n,b,m) – raw radiometry (DN) of detector element n of array b and gain m.

Y (n,b) - corrected radiometry (DN) of detector n of array b

C(n,b,m) – dark currents of the detector element n of array b for gain m

γ(b,m) – inter array equalization coefficient for array b and gain m

g(n,b) – equalization coefficient for detector element n of array b

These parameters must be available for all bands and detectors. They depend on the configuration gain value and the spectral band.

The calibration coefficients were obtained only for the lowest gain of the WFI OEB (x1) and only for two illumination levels. The illumination levels were adjusted in order to obtain output DN values around 100 and 200. The calibration coefficients are available in the document CBS-ITRP-113.

After getting the calibration data obtained in field campaign it is interesting to compare them with those one obtained in laboratory .

Absolute calibration

Absolute calibration parameters were obtained in laboratory for two illumination levels, which are presented in and Table 2.1.

Table 2.1 – Absolute calibration for WFI camera.

OEB SN03 Radiometric Calibration Parameters:

Absolute Radiometric Calibration must be used after relative calibration	LEVEL ~ 100 LSB				LEVEL ~200 LSB			
	Radiometric Calibration				Radiometric Calibration			
	B1L	B1R	B2L	B2R	B1L	B1R	B2L	B2R
	0,051		0,079		0,051		0,079	
	W/m2SrLSB		W/m2SrLSB		W/m2SrLSB		W/m2SrLSB	

3. IRMSS camera

The IRMSS operates in 4 spectral bands, thus extending the CBERS spectral coverage up to the thermal infrared range. It images a 119.5 km swath with the resolution of 77.8 m (156 m in the thermal channel). In 26 days one obtains a complete Earth coverage that can be correlated with the images of the CCD camera. It covers four spectral bands: B6: 0.50 - 1.10 µm (pan) ; B7: 1.55 - 1.75 µm ; B8: 2.08 - 2.35 µm ; B9: 10.40 - 12.50 µm.

Absolute calibration

The calibration data are already available, but unfortunately there is no information about the detectors filter functions. Therefore, it is not possible to calibrate the data without them.

Radiometry

Two points were observed:

1. B6 presents spectral band out of specification (spectral curves ?).

2. MTF values are lower than the values defined in the camera project (MTF > 0.4 in the Nyquist frequency). These values are:

   B6 = 0,3775

   B7 = 0,3611

   B9 = 0,3623 .

4. Conclusions

Unfortunately, the simple application of CCD calibration coefficients has not been sufficient to ensure all images with good quality. In some cases the inter-arrays calibration or in the overlap regions (S12 and S23) are not satisfactory.

The absolute calibration coefficients obtained in August resulted in a better target spectral characterization. Of course, once converted, the images can be converted in surface reflectance by the application of any atmospheric correction model. Improvements have also been done in 5S and 6S atmospheric correction models in order to accept CCD data and that conversion soon will be possible.

It is strongly necessary that these coefficients are now exhaustively evaluated in application studies. It is important to emphasize that they were determined in conditions in which neither all optimum assumptions were followed, mainly

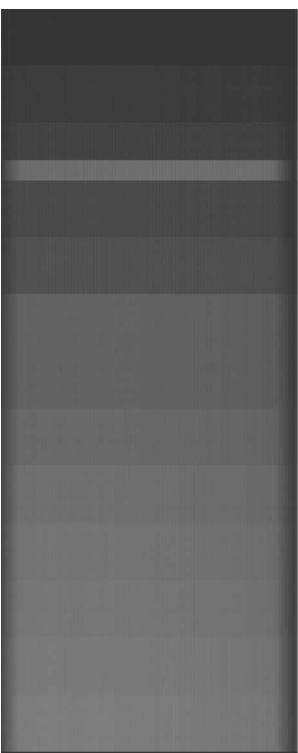that related to the bright of the reference surface. Methodological errors need to be identified and new solutions need to be developed.
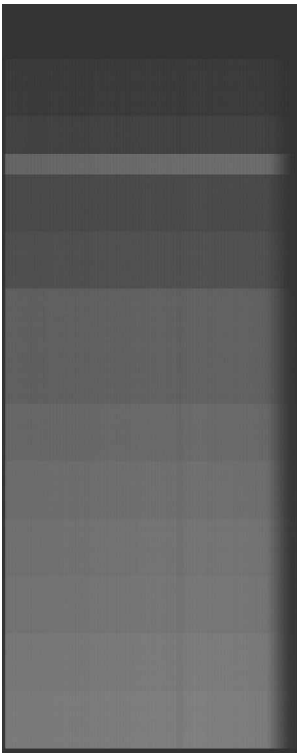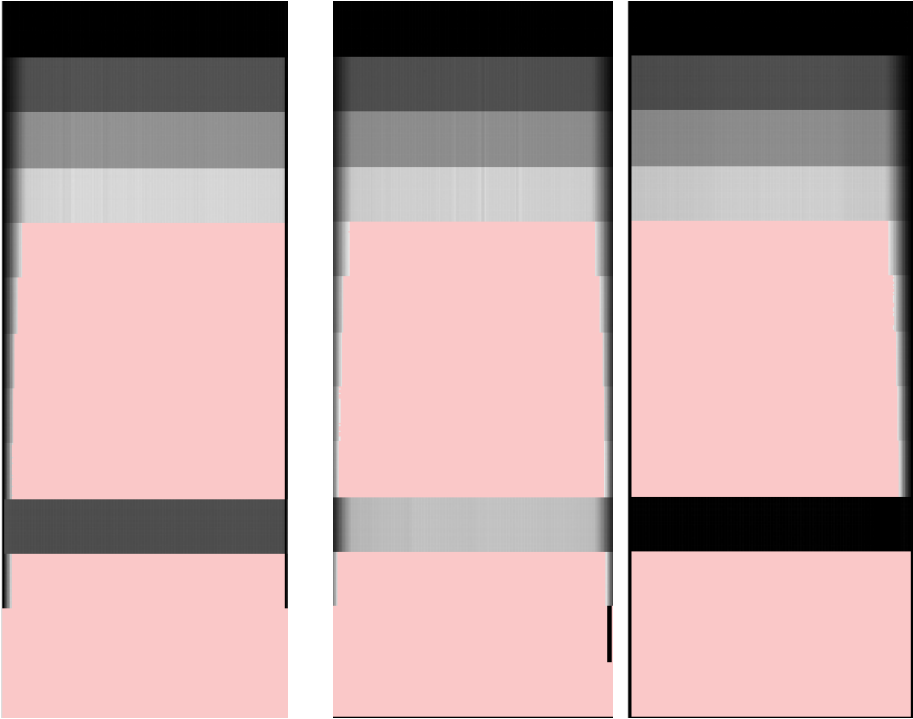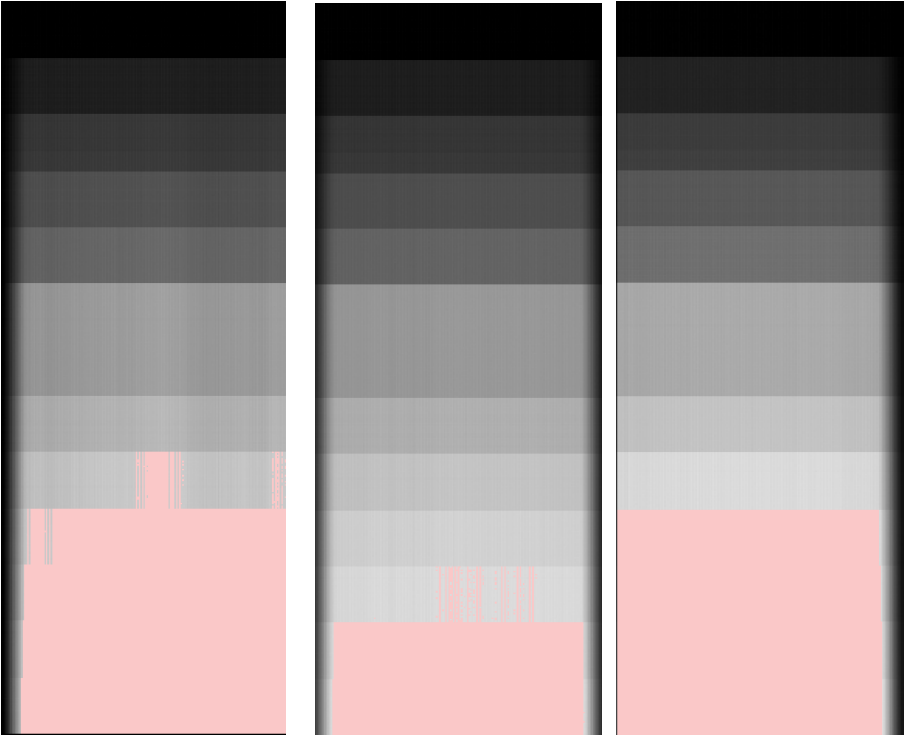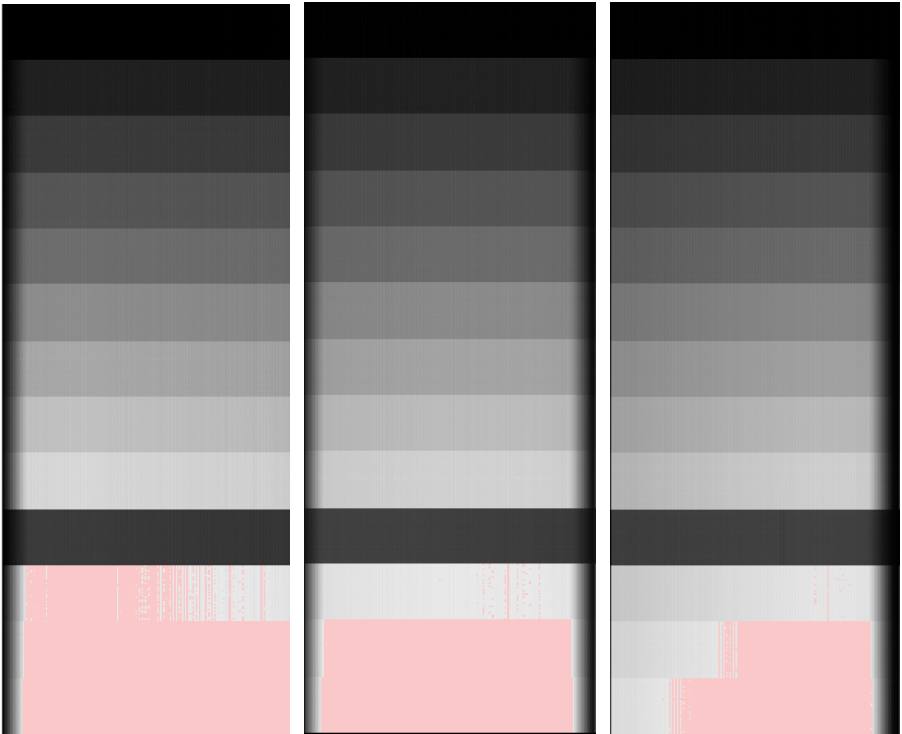
Appendix

Band 1
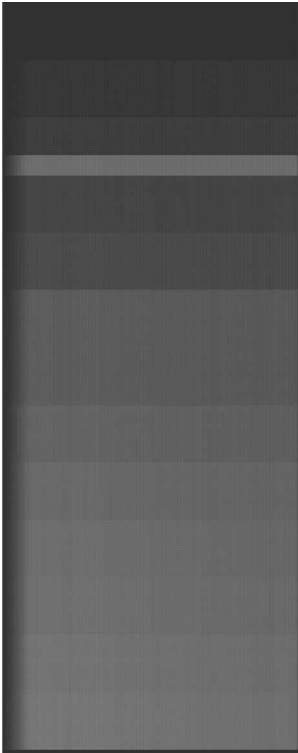
array 1   array 2   array3

Banda 4

Banda 3

Banda 2

Banda 5